Smartphone-Based SpO_2 Measurement by Exploiting Wavelengths Separation and Chromophore Compensation

NAM BUI, ANH NGUYEN, PHUC NGUYEN, and HOANG TRUONG, University of Colorado Boulder, Boulder, Colorado
ASHWIN ASHOK, Georgia State University, Atlanta, Georgia
THANG DINH, Virginia Commonwealth University, Richmond, Virginia
ROBIN DETERDING, Children's Hospital Colorado, Aurora, Colorado
TAM VU, University of Colorado Boulder, Boulder, Colorado

Patients with respiratory diseases require frequent and accurate blood oxygen level monitoring. Existing techniques, however, either need a dedicated hardware or fail to predict low saturation levels. To fill in this gap, we propose a phone-based oxygen level estimation system, called PhO_2, using camera and flashlight functions that are readily available on today's off-the-shelf smartphones. Since the phone's camera and flashlight were not made for this purpose, utilizing them for oxygen level estimation poses many difficulties. We introduce a cost-effective add-on together with a set of algorithms for spatial and spectral optical signal modulation to amplify the optical signal of interest while minimizing noise. A near-field-based pressure detection and feedback mechanism are also proposed to mitigate the negative impacts of user's behavior during the measurement. We also derive a non-linear referencing model with an outlier removal technique that allows PhO_2 to accurately estimate the oxygen level from color intensity ratios produced by the smartphone's camera.

An evaluation on COTS smartphone with six subjects shows that PhO_2 can estimate the oxygen saturation within 3.5% error rate comparing to FDA-approved gold standard pulse oximetry. In addition, our evaluation in hospitals presents high correlation with ground-truth qualified by the 0.83/1.0 Kendall τ coefficient.

CCS Concepts: • **Human-centered computing** → **Mobile computing**; • **Hardware** → *Sensor devices and platforms*;

Additional Key Words and Phrases: Oxygen saturation, optical divider, near-infrared sensing, skin colour compensation, heart rate variability, phone's add-on, phone camera, SpO_2, peripheral capillary oxygen saturation

This article is an extended version of the paper titled PhO_2: Smartphone-based Blood Oxygen Level Measurement Systems using Near-IR and RED Wave-guided Light, published in *Proceedings of the 15th ACM Conference on Embedded Networked Sensor Systems (SenSys'17)*.
This research is partially supported by the Schramm Foundation, the Colorado Advanced Industries Accelerator (AIA), and U.S. National Science Foundation grant #1602428.
Authors' addresses: N. Bui, A. Nguyen, P. Nguyen, H. Truong, and Tam Vu, University of Colorado Boulder, 1111 Engineering Drive, Boulder, CO, 80309; emails: {nam.bui, Ahn.TL.Nguyen, vp.nguyen, Hoang.Truong, tam.vu}@colorado.edu; A. Ashok, Georgia State University, 25 Park Place, Atlanta, GA, 30301; email: aashok@gsu.edu; T. Dinh, Virginia Commonwealth University, 401 W. Main St., Richmond, VA, 3019; email: tndinh@vcu.edu; R. Deterding, Children's Hospital Colorado, 13123 E 16th Ave, Aurora, CO, 80045; email: Robin.Deterding@childrenscolorado.org.

1550-4859/2020/01-ART9 $15.00
https://doi.org/10.1145/3360725

ACM Reference format:
Nam Bui, Anh Nguyen, Phuc Nguyen, Hoang Truong, Ashwin Ashok, Thang Dinh, Robin Deterding, and Tam Vu. 2020. Smartphone-Based SpO_2 Measurement by Exploiting Wavelengths Separation and Chromophore Compensation. *ACM Trans. Sen. Netw.* 16, 1, Article 9 (January 2020), 30 pages.
https://doi.org/10.1145/3360725

1 INTRODUCTION

Blood oxygen level, which is often indicated through oxygen saturation measurement (SpO_2), has long been recognized as an important indicator of patient's wellbeing and extensively used for clinical diagnosis [8, 23, 24, 35, 36, 60], owing to the critical role of oxygen in the operational functions of vital organs and tissues. If the human body cannot exchange and deliver oxygen efficiently, the amount of oxygen available for organs throughout the body becomes insufficient, which can lead to long-term damage of individual cells, heart, brain, and the like or short-term malfunctioning of other vital organisms [11, 33, 55]. Therefore, accurately measuring SpO_2 with high frequency is critical to not only monitor the key organ's well-being but also provide early warning signs of abnormalities and potential health problems. There have been extensive literature and commercial solutions both invasive and non-invasive to measure SpO_2. Pulse oximetry is a common measurement of SpO_2 for in-hospital and in-home environments. A typical noninvasive pulse oximetry system requires a dedicated pulse oximetry hardware and software [3, 7, 13, 15, 16, 37, 41, 43, 48, 56, 62]. The device projects light beams at specific wavelengths deep into its users' finger, toe, earlobe, or other location. Lights hit dedicated photo-electrodes after penetrating through multiple layers of skin, arteries, and blood cells. The electrodes are designed to receive only those within a desired wavelength range. The intensity of the received light carries the information that can be used to estimate the SpO_2 level of the blood cells that the lights have gone through [40]. While the current SpO_2 measurement largely relies on these dedicated pieces of equipment owing to their high accuracy and reliability, they have several undesirable features, especially for frequent measurement. First of all, users need to acquire the device by purchasing it (directly or indirectly through insurance or a doctor's prescription). Second, these pulse oximetry devices require users to carry the device with them for performing frequent measurements while they are doing everyday tasks (as opposed to being in the hospital). This requirement often reduces the usability of the devices since patients have tendency to forget their devices, fail to charge them, or misplace them [34]. Moreover, with the current form factors (e.g., finger clip-on, earlobe clip-on, or finger wrap-around), these devices do not always fit well on patients with different finger and earlobe sizes. For example, a 5-year-old boy would have a very different finger size with an adult and also have a different finger size when he turns 6. The ill-fitting of the device leads to significant estimation errors [13]. With the advent of smartphones, most of which are equipped with flashlights and cameras, many systems have been proposed using these functions to capture various blood properties [14, 18–20, 61]. However, none of the existing technologies and systems has the ability to accurately estimate SpO_2 by using built-in sensors in smartphones. For example, using external light sources such as an incandescent light bulb or a group of LEDs, HemaApp [62] from the University of Washington takes advantage of a clever machine learning technique to measure the hemoglobin concentration using the phone's camera. These additional light sources, however, are not pervasive and have restricted usage in modern smartphones, in which an IR filter is employed as part of the camera lens [22]. In addition, HemaApp attempts to estimate the hemoglobin count as opposed to estimating SpO_2. Existing works on estimating SpO_2 using the built-in flashlight and the camera of off-the-shelf smartphones include the systems proposed by Hodgkins et al. [15] and iCareOxygenMonitor [18]. However, all of them provide a very low accuracy and are not intended

for clinical use. More details about their performance is presented in the evaluation section (Section 8). The low accuracy is the result of the fundamental challenges when one tries to repurpose the camera and flashlight for SpO_2 measurement.

Challenges. First, most of the smartphone flashlights do not include the IR wavelength, which is a critical component for non-invasive SpO_2 measurement. Second, while most of state-of-the-art smartphone-based techniques are using a linear regression model to convert from pulsatile ratio to SpO_2 level, such a conversion does not work properly in practice due to the impact of the users' finger movements, pressure, contacting area, pulse amplitude, and ambiguity of converting from light intensity to RGB measurement of the camera. Third, the smartphone's camera picks up most of the lights from the flashlight including both hemoglobin responsive and hemoglobin non-responsive wavelengths. While the pulsatile is buried under a small intensity change of the hemoglobin-responsive light, this pick-up mechanism makes the collected light intensity of the camera non-usable for SpO_2 measurement. Fourth, the user's finger movement and finger pressure against the camera during measurement significantly affect the estimation quality. SpO_2 measurement relies on sensing user's pulsatile waveform whose amplitude is shorter than that of other human-generated movements. A tiny shift of our finger possibly magnifies the amplitude or even shatters the signal, which consequently has a significant impact on the prediction. Pressure control is as crucial as finger stabilization because strong pressure halts the blood flow in the arteries inside our fingertips. As a result, the pulsatile pattern disappears, leading to the measurement inaccuracy. Observation from commercialized pulse oximeters showed that the prediction will not be released if the input signal gets distorted. Instead, a warning message will show up to indicate the reason of the poor signal. Conventional wisdom has not yet distinguished between the motion of the finger and inadequate pressure. In most of the existing systems, users only receive a warning saying that their finger is out of the region, which makes it difficult for users to adjust the pose of their finger or modify how hard they should press on the camera. Fifth, we are concerned that the heat released by the phone's flashlight can cause a serious skin burn when shining on the finger for a long time. Note that, children's skin can quickly absorb the heat and gets burned under the high-intensity light source. Shortening the time of keeping the light on can help to reduce the heat, but degrades the signal quality, especially in the case of the reflectance mode where lights need to bounce back multiple times before hitting a receiver.

In this article, we propose a novel mobile oxygen saturation measurement system, named PhO_2, that has a potential to accurately provide the SpO_2 level in real time using the smartphone's camera and flashlight. Specifically, as demonstrated in Figure 1, PhO_2 is a phone-based system that includes a hardware add-on designed with optical filters of different wavelengths and snapped on the phone as simply as using a phone case. By leveraging the advancement of 3D printing technology and off-the-shelf filters, our add-on is lightweight and does not affect normal functionality of the phone's flashlight or camera. Moreover, PhO_2 produces two light beams at separate wavelengths from single light source with the use of the add-on. The add-on also helps stabilize the user's finger during the SpO_2 measurement and does not prevent the phone's camera from its normal use of taking pictures. However, due to limitations of camera hardware, the reflected light captured by the PhO_2 device needs to be further processed using dedicated algorithms to obtain usable PPG signals and reliably estimate the SpO_2 level. In particular, PhO_2 real-time model takes streamed frames to evaluate the appearance of possible artifacts and extract the PPG signal of high quality. The high-quality signal is finally input into a regression-based optimization model to calculate the SpO_2 level.

We made the following contributions in realizing the proposed PhO_2, a phone-based SpO_2 level estimation system:

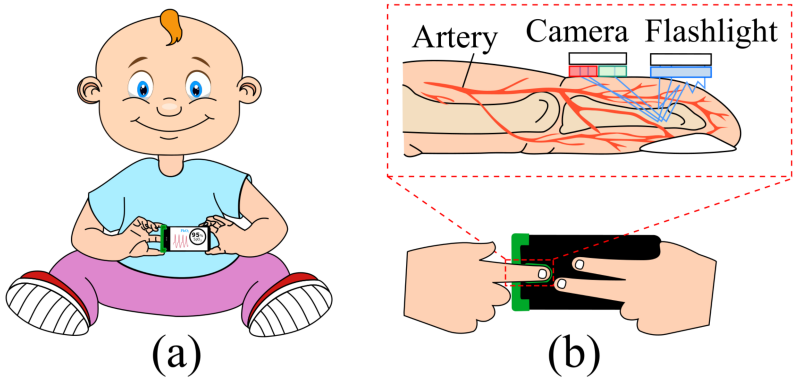

Fig. 1. PhO_2 and its general view for SpO_2 measurement. (a) A person is placing his index finger on PhO_2 add-on to check his SpO_2 level. (b) A back view of PhO_2 use in which the add-on covers the phone's flashlight and back camera and a zoomed-in visualization of how PhO_2 works.

- We develop a lightweight, cost-effective, and portable smartphone add-on allowing mobile device to measure SpO_2 level accurately and reliably.
- We propose an optical spatial separation technique to extract near infrared (NIR) and red lights from the camera's flashlight. As the NIR and red lights are hemoglobin responsive, their intensity variations are analyzed to infer SpO_2 ratio.
- We devise algorithms to identify the human motion artifact and pressure estimation that provide the best performance of PPG estimation and therefore improve the accuracy of SpO_2 measurement.
- We design a non-linear calibration technique to infer the SpO_2 level from the observed intensity from two separated lights mentioned earlier.
- We introduce an effective design for light distribution to reduce the heat load without affecting the light intensity.
- We verify the performance of our proposed solution with the gold standard noninvasive SpO_2 measurement device. The PhO_2 obtains 3.5% of accuracy with 80% of confidence compared the gold standard device with in-lab experiment. For the experiment conducted in the hospital, our device is highly correlated with ground-truth with Kendall $\tau = 0.83$.
- We confirm that the PhO_2 device receives very positive feedback from 12 trial users, including 6 members in the lab and 6 patients in the hospital.
- We discuss potential applications of our proposed technique. In particular, we envision that the spatial-optical dividing techniques can be used to extract the desired wavelengths for any light-based applications.

2 RELATED WORK

In this section, we present a thorough survey of existing literature on SpO_2 estimation to compare and contrast with our proposed system, PhO_2.

Pure Phone-Based Solutions. Multiple systems for easy-to-access oxygen-level measurement have been developed in the form of a mobile app. Existing apps, such as Instant Pulse Oximeter [19], Vigor SpO_2 [61], Instant Pulse Rate [20], Heart Rate Pulse Oximeter [14], and iCare Oxygen Monitor [18], follow the same schema in which a single streaming video clip with duration from around 10 to 15 seconds is processed to extract the heartbeat and oxygen level. The key shortcoming of these systems is their inaccuracy due to the challenges that we have mentioned in the previous

section. PhO_2, in contrast, identifies and addresses these challenges to significantly improve its performance.

Hardware-Aided Phone-Based Alternatives. The most relevant technique to our work is HemaApp [62], which uses a mobile phone camera with the aid of a high-power incandescent light bulb or a group of LEDs attached to the front of the camera lens, to measure the hemoglobin concentration but not the SpO_2 level. Although the system was cleverly designed and reportedly works well to estimate hemoglobin concentration, it strictly depends on the availability of an external IR light source and relies on the ability to capture the IR light of the phone's camera, which is not available in off-the-shelf devices with IR filter (we empirically prove this with the evidence of spectrum analysis of lights collected from iPhone 4, Galaxy S4, Galaxy S5, and Note 3 in the next section). Our system, in contrast, is not only free of hard-to-access additional equipment, but also independent of external IR source, which makes our app compatible with most of off-the-shelf smartphones.

Dedicated Pulse Oximeters. Pulse oximeters have been developed and widely used since 1930s. The designs and products have evolved from devices which are large, heavy, expensive, and available only for military and sleep laboratories [44] to ones that are cheap, small (ear-lobe usage [3, 13, 41, 43], fingertip compatible), and pervasive (e.g., FDA-approved devices can be bought easily from $30.00 [7, 16, 37, 48, 56]). There are also different form factors of pulse oximeter such as forehead-type [2, 4, 9, 51, 64], tracheal-type [5], and ring-type [17]. At the moment, the quality and performance of cheap pulse oximeter still raise concerns for the healthcare community [30]. Other dedicated hardware that can be connected to smartphones includes Phone Oximetry [45] and audio-based pulse oximetry [46]. They use the commercial pulse oximetry probe in connection with software on smartphones to calculate the SpO_2 level. However, these solutions require dedicated hardware to be purchased; users to carry the hardware with them for frequent monitoring; and sometimes the hardware does not fit the patient's finger or earlobe, which reduces its accuracy. In comparison, PhO_2 frees the users from carrying an additional device and allows them to use their mobile phones instead while maintaining the high level of accuracy.

Finger Pressure Detection and User Guidance Studies. Research on phone-based SpO_2 measurement [28, 53] or oxygen concentration (HemaApp) [62] left the problem of finger posture and inappropriate pressure remains untouched. However, in clinical literature, Hayes and Smith [12] points out that finger pressure is one of the main causes of error in pulse oximeters. Therefore, with PhO_2, the pressure at the contact area is carefully considered. A set of algorithms is proposed to estimate the improper pressure events from which a feedback is launched to notify users and to suggest pressure adjustment to users. To the best of our knowledge, pressure control has not been explored to improve signal acquisition for SpO_2 measurement for neither phone-based nor dedicated-hardware solutions. The techniques derived here, therefore, can benefit the current design of commercial dedicated-pulse oximeters as well.

3 PRINCIPLE OF SPO_2 MEASUREMENT

In this section, we present in detail the background of noninvasive oxygen saturation (SpO_2) measurement from its first principles, through derivation, to the practical techniques. This section sets the foundational understanding of the existing SpO_2 estimation techniques, from which PhO_2 is built up on.

Oxygen saturation (SpO_2) is the percentage of oxygen in arterial blood measured by taking a ratio of the hemoglobin with oxygen to the sum of oxide hemoglobin and dioxide hemoglobin. Therefore, SpO_2 level can be obtained by $SpO_2 = \frac{\rho_{02}}{\rho_{02}+\rho_{Hb}}$ in which ρ_{02} and ρ_{Hb} are the concentration of hemoglobin with and without oxygen, respectively. In an invasive SpO_2 estimation approach, ρ_{02} and ρ_{Hb} can be calculated through a blood gas test in which blood samples are

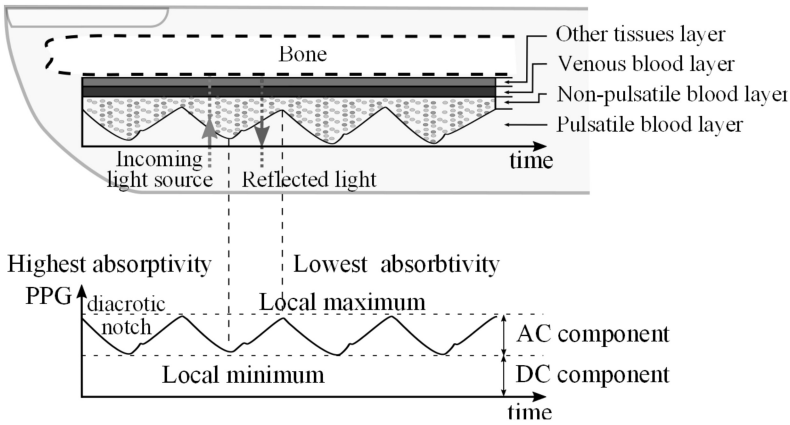

Fig. 2. Non-invasive SpO_2 measurement illustration in which an incoming light source penetrates different layers of a finger then reflects back to produce a PPG signal that is captured by a dedicated photoreceivers

collected and count the number of hemoglobin-binding oxygen [21]. Though this technique is accurate, it is invasive and costly. Therefore, non-invasive alternatives have been proposed and are much more widely used.

Non-Invasive SpO_2 Measurement. The key idea is to evaluate the attenuation of light penetrating through multiple layers inside the human finger and mark down the "pulsatile" waveform on a photon detector. This method is called photoplethysmography (PPG), which was originally developed as an alternative to measure cardiovascular pulse waves.

(1) How Is Pulsatile Wave Captured? The human finger includes multiple layers such as skin, pulsalite blood layer, venous blood layer, other tissues layer, and the bone (as illustrated in Figure 2 (top)). When a light beams into the finger, the reflected component, which can be captured by photodiode, has different intensity as shown in Figure 2 (bottom). The fluctuating patterns in the light intensity are caused by the following characteristics: (1) the local minimum value of the light's intensity, called *DC component*, represents the intensity of light that is reflected from the static component inside human fingers, such as bone, venous blood layer, and non-pulsatile blood layer; and (2) the maximum variance of the reflected light intensity, called *AC component*, is defined by the variance of the pulsatile blood layer. Using the latter characteristic, the variance of the reflected signal intensity directly correlates to the pulsatile waveform generated by cardiovascular waves [40].

Let's consider the beaming light that has the intensity of I_0 and the intensity of the reflected beam is I, the decrease of the intensity can be obtained from Beer-Lambert's law [31] using the following equation: $I = I_0 e^{-\varepsilon(\lambda)\rho d}$. In that, $\varepsilon(\lambda)$ is the absorptivity—a function of wavelength—and c and d are the concentration and depth of the medium, respectively. When light traverses through multiple media, the total absorption is the summation of all the media coefficients in the exponential term $I = I_0 e^{\sum_i -\varepsilon_i(\lambda)\rho_i d_i}$.

Considering oxyhemoglobin, deoxyhemoglobin, and tissues as the three main media inside the finger that let light traverse through, the light intensity after reflection can be represented as:

$$I = I_0 e^{2(-\varepsilon_t(\lambda)\rho_t d_t - \varepsilon_{Hb}(\lambda)\rho_{Hb} d_a - \varepsilon_{02}(\lambda)\rho_{02} d_a)} \tag{1}$$

In that, ε_t, ε_{Hb}, and ε_{02} represent the extinct coefficients of other tissues, pulsatile, and non-pulsatile blood layers, respectively. d_t and d_a denote the thickness of tissue and blood medium, respectively. The key factors are the concentrations denoted as ρ_t, ρ_{Hb}, and ρ_{02}, respectively to

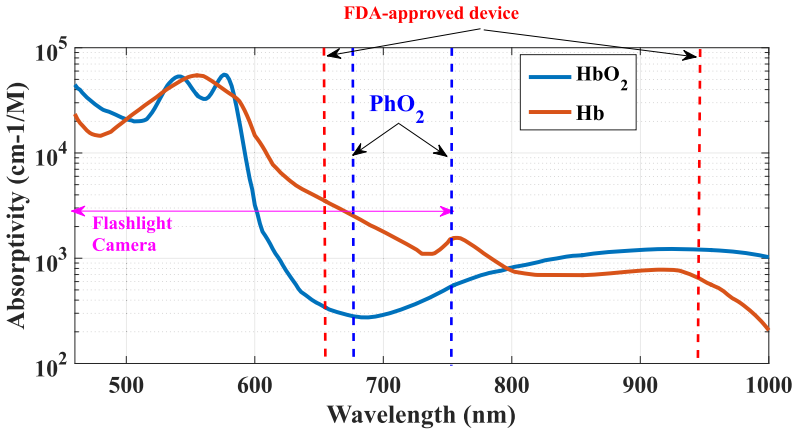

Fig. 3. Absorptivity of hemoglobin and dehemoglobin versus wavelengths.

each medium. The optical path length of tissue layer d_t might be stable while arterial part d_a varies periodically following cardiac activities. Therefore, the light intensity received when the blood level is at minimum (in diastolic phase (d_a^s)) and at maximum (in systolic phase (d_a^e)), denoted as I_p and I_b, can be presented as:

$$I_p = I_0 e^{2(-\varepsilon_t(\lambda)\rho_t d_t - \varepsilon_{Hb}(\lambda)\rho_{Hb} d_a^s - \varepsilon_{02}(\lambda)\rho_{02} d_a^s)} \tag{2}$$

$$I_b = I_0 e^{2(-\varepsilon_t(\lambda)\rho_t d_t - \varepsilon_{Hb}(\lambda)\rho_{Hb} d_a^e - \varepsilon_{02}(\lambda)\rho_{02} d_a^e)} \tag{3}$$

Taking the ratio of I_p and I_b, we obtain the form in which some of the variables are called.

$$\frac{I_p}{I_b} = e^{-2(\varepsilon_{Hb}(\lambda)\rho_{Hb}(d_a^s - d_a^e) + \varepsilon_{02}(\lambda)\rho_{02}(d_a^s - d_a^e))} \tag{4}$$

The absorptivity change can be obtained by taking the natural logarithm of the above equation and scale by half $A = 0.5ln(\frac{I_p}{I_b}) = \varepsilon_{Hb}(\lambda)\rho_{Hb}\Delta d_a + \varepsilon_{02}(\lambda)\rho_{02}\Delta d_a$, where $\Delta d_a = d_a^s - d_a^e$ is another unknown variable. To remove this value, we apply the formula for one particular wavelength. In the commercialized pulse oximeter, the wavelengths corresponding to Red and IR are selected to calculate the absorptivity ratio (Figure 3) [27, 52, 68]. We can rewrite the following equation to take redundancy factors into consideration.

$$A = \varepsilon_{Hb}(\lambda)\rho_{Hb}\Delta d_a + \varepsilon_{02}(\lambda)\rho_{02}\Delta d_a + A_\eta \tag{5}$$

Finally, we derive the form of the differentiation absorbtivity as follows:

$$\frac{dA}{dt} = \varepsilon_{Hb}(\lambda)\rho_{Hb}\frac{\Delta d_a}{dt} + \varepsilon_{02}(\lambda)\rho_{02}\frac{\Delta d_a}{dt} \tag{6}$$

$$\begin{aligned} R &= \frac{d\left(ln\left(\frac{I_p(r)}{I_b(r)}\right)\right)/dt}{d\left(ln\left(\frac{I_p(ir)}{I_b(ir)}\right)\right)/dt} \approx \frac{\frac{I_p(r)-I_b(r)}{I_b(r)}}{\frac{I_p(ir)-I_b(ir)}{I_b(ir)}} = \frac{\frac{AC(r)}{DC(r)}}{\frac{AC(ir)}{DC(ir)}} \\ &= \frac{\varepsilon_{Hb}(r)\rho_{Hb} + \varepsilon_{02}(r)\rho_{02}}{\varepsilon_{Hb}(ir)\rho_{Hb} + \varepsilon_{02}(ir)\rho_{02}} \end{aligned} \tag{7}$$

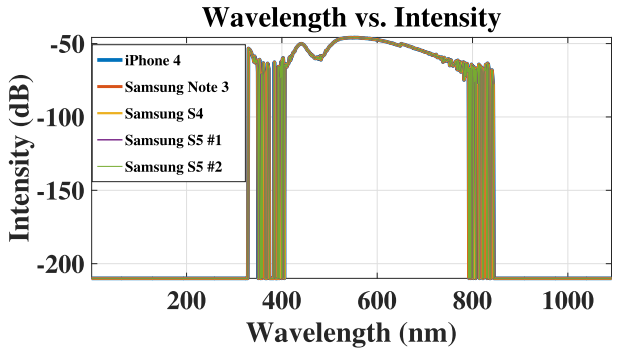

Fig. 4. The intensity of different wavelength generated by flashlight from different smartphones.

Recall that the measurement of SpO_2 is calculated by $SpO_2 = \frac{\rho_{02}}{\rho_{02}+\rho_{Hb}}$. By substituting ρ_{02} and ρ_{Hb} into Equation (7), we first isolate the term:

$$\rho_{02} = SpO_2(\rho_{02} + \rho_{Hb}); \rho_{Hb} = (1 - SpO_2)(\rho_{02} + \rho_{Hb}). \tag{8}$$

Hence, Equation (7) after the replacement becomes:

$$R = \frac{\varepsilon_{Hb}(r)(1 - SpO_2) + \varepsilon_{02}(r)SpO_2}{\varepsilon_{Hb}(ir)(1 - SpO_2) + \varepsilon_{02}(ir)SpO_2} \tag{9}$$

By exchanging the position of absorptivity r and SpO_2, SpO_2 can be derived from the following final formula:

$$SpO_2 = \frac{\varepsilon_{Hb}(r) - \varepsilon_{Hb}(r)R}{\varepsilon_{Hb}(ir) - \varepsilon_{Hb0_2}(r) + [\varepsilon_{Hb0_2}(ir) - \varepsilon_{Hb}(ir)]R} \tag{10}$$

(2) Why Do We Need Two Wavelengths? The typical hardware of the pulse oximeter includes two light sources (Red and IR wavelengths) at the transmitter side. On the receiver side, two photon detectors are used to measure the intensity of the two lights after going through our finger (transparent type) or reflecting at the contact point (reflectance type). When using the flashlight and camera as transceivers, the transmitter and receiver are placed on the same side. In human blood, the majority of hemoglobin components (called *functional hemoglobin*) are oxygenated hemoglobin (oxyHb) and deoxygenated hemoglobin (deoxyHb) (around 98%); the other 2% (called *dysfunctional hemoglobin*) includes metHb and coHb. Those two components absorb an unequal amount of light at different wavelengths. In order to measure the oxygen saturation level, the two wavelengths must be used to compare how much of each light is absorbed by blood. Depending on the amount of oxyHb and deoxygenated Hb present, the ratio of amount of the first light absorbed compared to the amount of the second light absorbed will be obtained and inferred the SpO_2 level.

(3) Which Wavelengths Are Used? In traditional pulse oximeter design, RED light (660 nm) and near-infrared (IR) light (940 nm) are used to maximize the differences between absorption level of oxygenated and deoxygenated hemoglobin. However, IR lights are not producible by smartphone's flashlight and its camera cannot capture the light at IR frequencies. Indeed, our spectrum analysis results for flashlight of various phones (iPhone 4, Galaxy S4, Galaxy S5, and Note 3) show that there is no IR components in the flashlight (Figure 4). Furthermore, most of latest camera lens come with built-in IR filter for improving normal picture quality, which makes it impossible to record IR light in off-the-shelf phone. Due to those difficulties, our system must be able to select the two lights with the most appropriate wavelengths that works with smartphones while giving the recognizable absorption ratio between oxygenated and deoxygenated hemoglobin.

All in all, to measure SpO_2 level accurately from off-the-shelf smartphones, the system needs: (1) two different hemoglobin-responsive light sources; (2) these two lights must be spatially separated so that the receiver can distinguish their impact on the camera sensor; (3) the camera has to be able to infer from the intensity to the pulsatile variance for SpO_2 measurement; and (4) The obtained pulsatile must be usable for properly inferring SpO_2 measurement regardless of changing subjects or smartphones.

4 SYSTEM OVERVIEW

In this section, we first present the challenges in realizing PhO_2, then discuss different components of the system that are designed to address these challenges.

4.1 Design Challenges

(1) Smartphone's Flashlight Cannot Generate IR Lights. In literature, Red and IR light are the two wavelengths that yield the highest accuracy and are used in most FDA-approved noninvasive pulse oximeters (see Section 3). However, since the camera's flashlight is made to generate lights that are capturable by the camera, the light that it produces is manufactured so that it falls only within the visible range. To confirm this phenomenon, we conducted an experiment to analyze the wavelength of lights from modern smartphones (including the Galaxy Note 3, Galaxy S5, Galaxy S4, and iPhone 4). We used Ando Model AQ6315E Optical Spectrum Analyzer [42] for this experiment. The result in Figure 4 shows that the flashlight contains only the light within the visible and near IR ranges (wavelength from 400 nm to 779 nm). To overcome this problem, instead of selecting the Red and IR lights as in the ideal cases, we make use of the Red wavelength (670 nm to 690 nm) and near IR (NIR) wavelength (700 nm to 779 nm) from the flashlight (see Section 5). This modification requires a new model for us to identify the wavelengths that work best. We present our wavelength selection technique in Section 5.

(2) NIR Filter Needs to be Thin. To construct our add-on, the filter must be thin enough to avoid signal loss due to optical absorption and scatter. However, there is no NIR filter on the market that fits our need due to its minimum thickness. The minimum thickness that we found for NIR filter is usually around 5.1 mm [39]. We propose to take advantage of the non-linearity of the basic color filter (green color) to address this problem, as can be seen later in Section 5. As a result, our designed filter has the thickness of less than 1.5 mm, which is suitable for most mobile add-on form and minimizes the distance between the human finger, the light source, and the camera.

(3) Smartphone Camera Is Noisy. The smartphone camera is designed to pick the light component that has high intensity within the visible range. It usually gathers the whole range of transmitted white light from the flash. Hence, the light intensity variance captured by the camera after going through user's finger is very noisy due to the impact of non-responsive hemoglobin wavelengths. A light divider and a set of separation algorithms are required to create two separated light sources for SpO_2 measurement (see Sections 5 and 6).

(4) Human Finger Pressure Has Significant Impact to the Accuracy Measurement. The ratio between the two light sources helps to remove the impact of non-AC component. However, given the sensitivity of the camera sensor, the pressure of placing the human finger as well as the size of the contacting point plays an important role to the accuracy of estimation. The finger movement and pressure have a large impact to the accuracy of measurement. Therefore, online feedback system is needed to make sure that the finger movement does not happen during the experiment and the user provides sufficient pressure to the device (see Section 6.1).

(5) Impact of Red Chromophore on the Stability of the Measurement. The dominant color in the captured image is red which directly relates to the red chromophore of skin, flesh, and the hemoglobin layer. In the existing techniques of using LEDs with single-wavelength, the variation of red

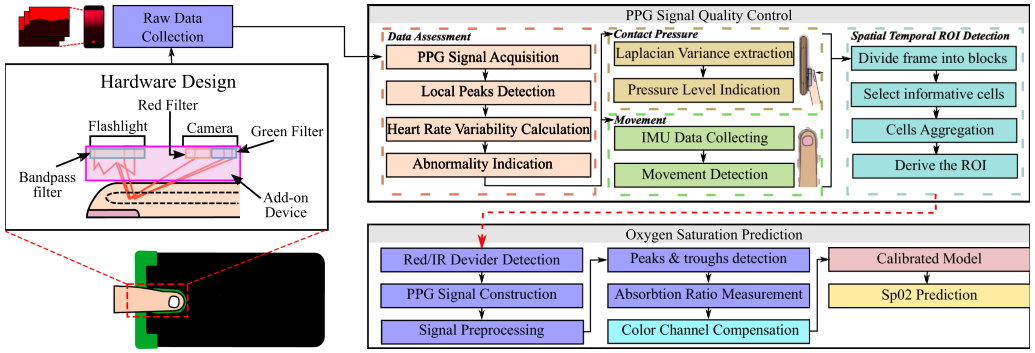

Fig. 5. Overall system design and architecture of PhO_2.

chromophore produces less interference to the primary receiver and can be considered as one participant in the DC component. Camera sensors usually capture a wide range of wavelengths, thus, magnify the errors. The conventional wisdom on removing DC is not sufficient to eliminate the impact of red chromophore variation. Therefore, we introduce an extension of the formula for the absorptivity R to further remove the constant factors such as red chromophore. By adjusting the gain parameter in the compensation term, it is possible to evaluate the effectiveness of the proposed solution (see Section 5).

(6) Legacy Linear Regression Model for Light Intensity to SpO_2 Is not Applicable. Linear regression model is applied for most of pulse oximeter devices as the light beams (photo diodes) and photodetectors are specifically designed for SpO_2 measurement [59]. When using the flashlight and camera from the phone, the linear regression model cannot be used due to the impact of the flashlight's noises (non-responsive hemoglobin wavelengths) and the light intensity to RGB conversion, the human pressure, contacting area, and finger movements to the camera's readings. Therefore, the SpO_2 calculation model must take all these effects into account (we propose a new mapping model for the camera-based method in Section 7).

(7) Preventing Skin Burn Caused by Concentrated Lights. Energy from the lights can convert into heat and results in blister burns on skin. To the best of our knowledge, none of the research about measuring vital signals using the phone flashlight discusses this issue. We also did not notice the problem at the first stage of this project [6] until it had undergone a series of user evaluations in the hospital to reveal the burning issue as a serious problem that needs to be solved first to protect future users. Reducing light intensity is not an option because it will affect to the quality of PPG signal. Using our proposed design of light distribution as described in Section 5, we show that the temperature drops significantly below the minimum threshold of burning skin.

4.2 Proposed System

In this section, we outline the structure of our system in measuring the oxygen level by adapting only the parts and functions built in to the off-the-shelf smartphone, as illustrated in Figure 5. The specific design of add-on helps to isolate the lights with two different wavelengths. The raw data is recorded and segmented before undergoing multiple steps of processing to give out the final prediction. On top of that is a mechanism that helps to ensure that the quality of the signal is not affected by motion artifacts and inappropriate pressure.

Optical Spatial Divider for Wavelength Separation. Unlike the lights in an incandescent lamp, the lights coming from the flash in a smartphone do not contain components whose wavelength is larger than 780 nm. The current pulse oximeter relies on the lights that reach the IR frequency,

which is unobtainable when the flashlight is the only source of illumination. We can use the fact that the outer sources were from external components such as LED or incandescent lamps, which was introduced in HemaApp [62]. Then power is an issue. In order to use only the flashlight source, it is essential to select a substitute wavelength for IR in the range that is given by the smartphone flashlight. The lights with wavelengths less than 600 nm will be absorbed by the red skin pigmentation. Therefore, our interest range is from 600 nm to 779 nm and the one that maximizes the angle of relational curve between Red and IR (figure) is our candidate. The arrangement of one optical polyester filter and a narrow-band borosilicate glass filter, following the two frequencies, on camera surface is our system's unique signature in dealing with wavelength separation and without the need of additional illumination sources. The structure is integrated within the add-on, including a special feature for the finger-stabilization, which attaches firmly to any smartphone fit to the design. In addition, the light distribution feature is purposely positioned in front of the smartphone flashlight to evenly share the intensity over the finger, and thus reduce the risk of getting burned.

Finger Pressure Control. While existing systems allow signals with motion interference to be pruned into their main functions, we argue that PPG signals are overwhelmed by other movements and thus cannot be completely separated. The design of PhO_2 will not take them into account; in fact, they need to be eliminated or utilized to inform users in advance of the struggle. The system can (1) differentiate between motion and the fluctuation from pulsatile nature within a small number of frames, (2) sense the pressure level by only vision features, and (3) notify users whether the signals are noisy and show an instruction to adjust their finger placement. The real-time function provides a more generic picture to interpret the respiratory conditions rather than getting the result after a specified minimum wait.

The prototype is supported by a set of multi-stage processes from manipulating with the raw data, smoothing, processing the outcome signal to the key features of the estimation of absorption ratio and its reference to the oxygen level. Each of the procedures critically contributes to the success of our prediction model. Here, we address every single piece of the system starting from the point that has been assumed for a long time to be trivial.

Red Chromophore Compensation. We realize that the impact of red chromophore overwhelms other factors. Therefore, in the extension form of absorptivity R, we try to isolate the red chromophore from the other DC components so that it can receive more special treatments. First, we remove the redundant information in the Red source by discarding the green factors in the red filter region. Similarly, the IR component is filtered by removing red factors in the green filter region. Then, to completely block the impact of the red chromophore, we further subtract the average of red intensities for each calculation of R.

Optimal Relational Model. Given the frequencies in that range without the IR, the variation of ratio R is small compared to the change of SpO_2 making the linear calibration becomes inaccurate. Since, the pulse oximeter adapts Red and IR lights, the relation between absorption ratio and R (Eq. (7)) can be approximated by a linear equation. We argue that using the original equation with a larger number of variables to map between R and measured SpO_2. In this article, we propose a solution to formulate the problem using descent gradient, to be more specific, the Levenberg-Marquardt [25] method helps to identify the best fitting curve for our model. The high saturation of the flashlight versus the dense and focus beam of LED diode returns a large number of outliers which defects the estimation. Our expectation is to select only the pairs, R and SpO_2, which contributes most to the regression curve. RANdom SAmple Consensus (RANSAC) is developed to divide the inliers and outliers of data points without any prior knowledge about the model. Using iterative cross-validation, RANSAC filters the outliers at each iteration and reserves only the meaningful data points. The hybrid structure of Lavenberg-Marquardt and RANSAC gives a strong

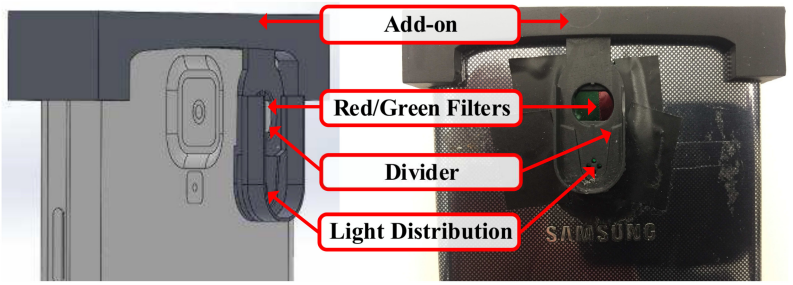

Fig. 6. PhO_2 hardware design (3D model - left, Prototype - right).

fitting curve which eliminates the outliers in the data and solves the high complexity problem such as the relation between SpO_2 which is a fractional equation with four degrees of freedom.

5 OPTICAL SPATIAL DIVIDER

In this section, we will introduce the design of add-on and discuss how the filters satisfy the non-invasive measuring prerequisites. From the Beer-Lambert law, the problem of light scattering is negligible, which does not reflect the real situation correctly. Moreover, the diffusion of the flashlight and other sources from the environment can reduce the system performance. To minimize the distortion, we designed a special add-on to (1) prevent the interference of unwanted components from the natural source, (2) navigate the light toward the camera region, (3) stabilize a finger during the recording session, and (4) play a role as a shield to protect the lens. Using SolidWorks [58] software for design and a 3D phone model, we created the add-on with specific features that can conveniently snap on top of the corresponding device and easily be removed for normal usage. Right above the camera region is the finger-stabilizer having a curve of the fingertip. This feature allows users to easily slide their fingers in and also leaves more space for lights to bounce off the finger and hit the camera lenses. The component also prevents the user from pressing too hard, which halts the bloodflow into their vessels, thus resulting in the failure to capture the pulsatile wave. The material is chosen to be the stiffest and manufactured with a very fine-grained resolution.

The two lenses are positioned to equally divide the image into two regions for Red and NIR, respectively, as illustrated in Figure 6. Following the Plank equation, NIR light has smaller energy than the visible one and thus needs long exposure time to leave a trace on camera sensor. The CCD function uses a pool of electrons to measure the intensity. Obviously, the visible light with its strong energy will have a better chance to fulfill that pool rather than the NIR. We placed a band-pass optical filter covering the flashlight to reduce the portion of visible components and allow for more NIR to come in and collide with the CCD sensor.

While most of color-filter is capable of blocking all the unwanted colors, the near IR component will always go through the color filtering. We design two filters and attach them to the smartphone's camera. The first filter absorbs the Red light at wavelength 680 nm (20 nm bandwidth) [1] and a green filter [29] to allow the near IR and green lights to pass through. The second filter removes the red component and only allows the light components that are highly absorbed by the red skin (wavelength less than 600 nm [57]) to pass through. Fortunately, the latter filter also allows the NIR light component to go through it. By carefully designing those two filters, we obtained two frequency components in the light (Red after the red filter and NIR after the green filter) as shown in Figure 8. The precise wavelengths need to be identified for the measurement of oxygen level. The research of Karlen et al. [26] about the correlation between SpO_2 and absorptivity ratio

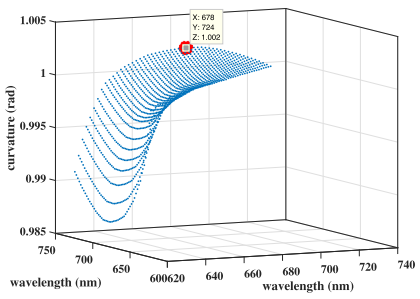

Fig. 7. The curvature level of different wavelength combinations.

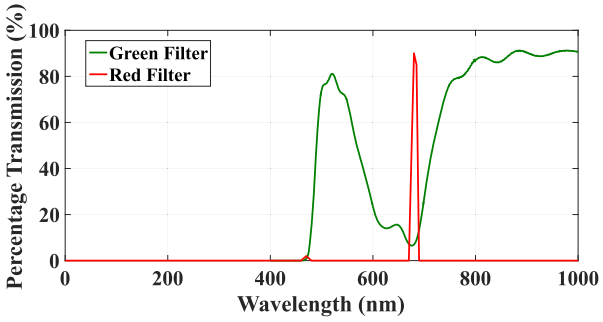

Fig. 8. Green/Red filter characteristics. The NIR is observable through the green filter while Red is blocked.

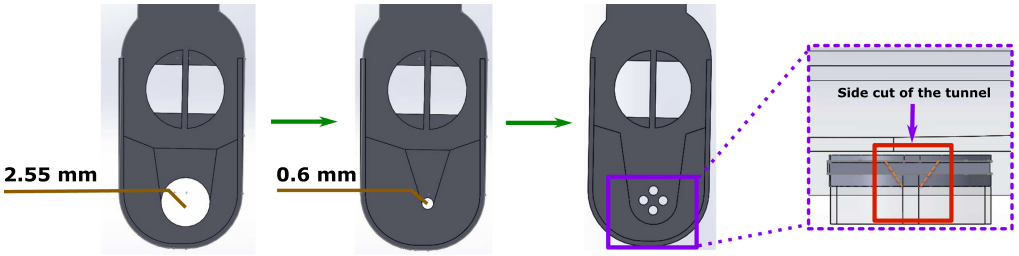

Fig. 9. The curvature level of different wavelength combination.

(R) with respect to different combinations of the light source indicates that the cultivation of the relational curve between SpO_2 and R can help to identify the wavelengths. The large angles have a better performance according to [26]. We replicate that simulation for those lights having wavelength from 600 nm to 750 nm and calculate the curvature level of angle between the relational curve and the vertical axis. From Figure 7, the combination of lights at 678 nm and 724 nm has the highest curvature at 1.002 radian. We select those as the possible candidates and search for all the neighbors to identify the optimal pair.

Alleviate Heat from the Smartphone's Flashlight Shining on the Finger. The previous design [6] did not encounter the heat issue since our evaluation did not remain unsolved long enough. In this version, we identify the problem and refine the structure to minimise the focused energy at one point. At first, we reduce the radius of light guiding tunnel from 2.55 mm to 0.6 mm, which also reduces the amount of intensity (Figure 9). To resolve the problem, additional tunnels are included, so that more light rays can pass through and only a small amount of energy is created in each tunnel. The design of light distribution can cut down a large amount of heat and retains sufficient intensity to capture pulsatile information and reduce light scattering.

6 PHOTOPLETHYSMOGRAPHY SIGNAL EXTRACTION

In this section, we present our solution for pressure correction, which is based on the fact that different levels of pressure can affect the the pulsatile shape. To further improve the quality by cutting off the uninformative areas within a frame, we introduce an algorithm to extract only blocks having a strong FFT peak that associates with the clear pulse rate.

6.1 Mitigating Impacts of User Behaviors

Influences to Signal Quality. As we stated in previous section, the PhO_2 system uses the non-ideal light source (phone flashlight) and receiver (recorded image frames) which has multiple drawbacks

and challenges. These include the uncontrollable light source (i.e., phone flashlight) and image captured from IR-filter-equipped off-the-shelf phone camera. Those two factors are highly sensitive to light channel interference between the flashlight and camera. Theoretically, our system must record reflected light from patients' finger at extremely close distance in order to extract the PPG signal from the stream of video. Thus, even a slight interference to the channel between the light source and receiver would cause certain consequence to the signal quality (i.e., reflected light and captured images). We investigated the abnormal changes in our PPG signal in order to search for the causes of interference. Based on recorded data from the subjects and their PPG signal analysis, we find out that the unavoidable sources of interference include (1) the subject's body movement, (2) miniature movement at the fingertip due to human organ activities, and (3) unawareness of the subject's finger pressure on the device.

First of all, human bodies are subjected to displacement of the breathing process. When inhaling or exhaling, the upper body parts (i.e., abdomen, chest, and shoulder) fluctuate at respiratory frequency. While measuring SpO_2, subjects follow the instruction to stabilize their finger on the device. However, at this so-called "stable" posture, the deltoid and pectoralis minor muscle groups keep moving the arm and hand back and forth slightly. Thus, a small displacement at the contact-point fingertip and the camera is generated, which leads to the abnormal change in the received PPG signal.

Second, each heartbeat, which ejects blood into the vessels, causes a repetitive motion in the human body. This phenomenon is called the *heart ballistic forces*, which can measured from the ballistocardiography (BCG) signal. These BCG signals can be easily observed by adding sensors to everyday objects or to the human body. Each blood pump cycle generates pulses that can be observed from all parts of the human body, even the fingertip in our case. Those pulses also create miniature changes at the contact point, which affect the intensity of the recorded frames. This leads to the abnormal patterns of the PPG signal.

Last, while using our system, the subjects were observed to change their pressure on the contacting point unconsciously. The digitorum profundus and flexor digitorum superficials muscle groups, which control the movement of fingers and fingertips, tend to move slightly even when the subject is at the stable and relaxed position. This causes the most influence on the surface at the finger and the flashlight/camera, in such cases inappropriate pressure causes the intensity of received signal to be overstimulated or too low. Fortunately, by analyzing the recorded frames, our system can successfully detect whenever the subjects' fingers are at the wrong degree of pressure.

Mitigate the Pressure Problem. Pressure detection has been addressed for the usage of mobile phone camera and flash [32]. In addition, motion artifacts and movement detection for the traditional PPG data collector and pulse oximeter have been proposed in [26, 65–67]. SpO_2 is designed with a pressure detection algorithm to deal with the problem when the subjects' fingers apply the force on the devices incorrectly.

In our previous prototype [6], different levels of pressure are identified by accessing the height of peak amplitude of the FFT transform processed in an N-second chunk of data [6]. We experienced that the FFT (1) is not robust to estimate motion and pressure and (2) is a costly computation. Therefore, we break the problem into two pieces. First, we detect the abnormality waveform, which indicates that either movement or inappropriate pressure happened. Second, based on the IMU data, we can precisely tell whether or not the movement occurs. If the answer is yes, a pop-up message will appear asking users to stabilize their fingers. Otherwise, it processes into the next stage for detecting pressure. Note that the system should be able to immediately inform users about how to adjust their pressing against the camera. That implies the procedure should take only a small number of frames in processing.

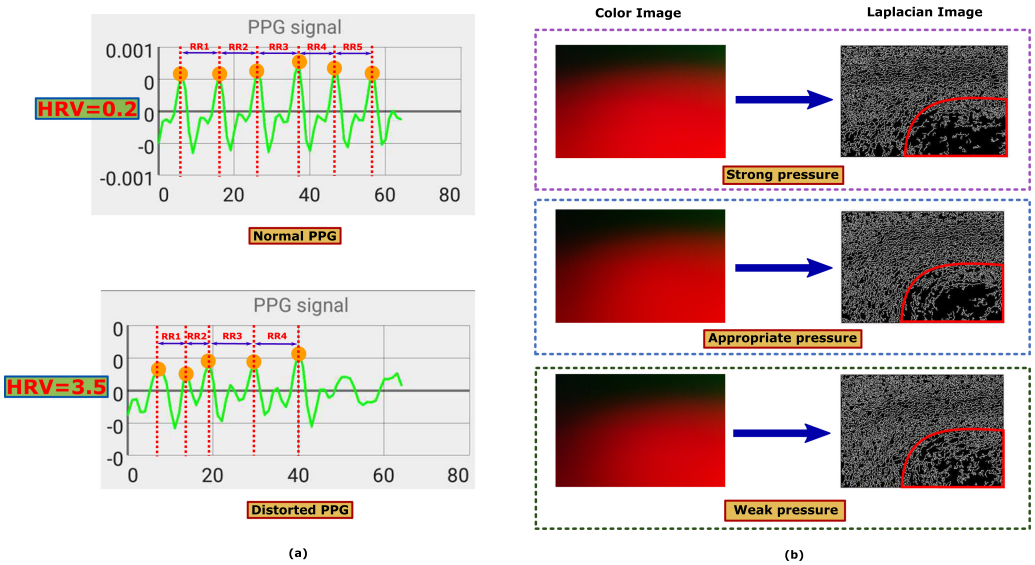

Fig. 10. PPG signal quality monitoring. (a) Abnormal PPG signal detection using Heart Rate Variability. (b) Pressure control using Variance of Laplacian Image.

The abnormal Heart Rate Variability is an indication for distorted PPG signal. To obtain the HRV, first, the duration between two consecutive PPG peaks is estimated to return the RR interval. Then, the standard deviation of all RR intervals within a chunk defines the HRV. Figure 10(a) illustrates the distorted PPG signal has large HRV than normal one (3.5 versus 0.2). In our application, the HRV threshold is at value of 2 to be sufficient to detect the distortion.

To process in each frame, we analyse the quality of the image associated with the pressure level. Fingerprint features are flattened under strong pressure, thus, the observed image looks blurred. When users loosen their fingers, the amount of details in the image increase because the fingerprint features pop out. Therefore, image smoothness can be used to infer the level of pressure of the finger pressing on smartphone's camera. The coarseness of a picture, defined by the number of edges and corners, can be evaluated using variance of the Laplacian image.

Laplacian image $L(x, y)$ is the second spatial derivative of a corresponding gray image $I(x, y)$: $L(x, y) = \frac{\partial^2 I}{\partial x^2} + \frac{\partial^2 I}{\partial y^2}$. The value of Laplacian at pixel (x, y) gives the information of the stiffness of surrounding area. Pixels belonging to the edges or corners in Laplacian image have a larger value than those in the smooth area. In total, a blurred image results in a lower variance of Laplacian than that of a coarse image. In Figure 10(b), three different pressing levels and their corresponding Laplacian images are demonstrated. As can be observed clearly in the region enclosed by the red boundary, strong pressure produces a smaller amount of details than weak pressure.

The algorithm can be minimized up to a 1-second window at 0.5 seconds overlap and still detect the wrong subjects' finger posture. By detecting the correct position of the bad pressure, our system smooths the extracted PPG signal and gets rid of the abnormal error calculation to the final result. Ideally, the system can scan for bad posture at the basis of every 0.5 seconds and notify to the subjects while measuring SpO_2 in real-time so that they can adjust the pressure by themselves.

6.2 ROI and Red-IR Divider Detection

Although the pressure is detected and provides an online feedback to the user, the contacting area between human finger skin and the camera filters are not even. We need to detect the region

ALGORITHM 1: Borderline detection using K-means clustering.

input: I- input image with the divider.
output: $ListId_k$ List index of pixels in each region.

Initialize values for the means of each region μ_1 and μ_2 respectively.
/* Finding optimal means and their corresponding list of pixels.*/
for $t = 1 \rightarrow MaxNumberOfIteration$ **do**
  $ListId_k \leftarrow []$;
  for $i = 1 \rightarrow NumberOfPixel$ **do**
    $\hat{k} = \text{argmin}_{k=\overline{1,2}} d(p(i), \mu_k)$;
    $ListId_{\hat{k}} \leftarrow [ListId_{\hat{k}}; i]$;
  end
  Update values for each μ_k
end
return $ListId_k$;

of interest at which the camera can capture the PPG signal properly and clearly. Typical size of pinhole camera is from 0.33 to 0.58 mm [47], which is too small to accurately manipulate. Since the divider is not always in the middle of the image, to precisely allocate the region for Red and NIR, a vision technique is required to subsequently split the two areas. Under the incandescent light, the two areas appeared with two different colors (red and green). The distance between two pixels p_i and p_j giving its chromatic characteristic is defined as $d(p_i, p_j) = \sqrt{\sum_{c=1}^{3}(p_i(c) - p_j(c))^2}$, where $p_i(c)$ indicates the intensity of pixel i in color channel c. The detection can be formalised as a segmentation problem which can be achieved by using the K-means clustering (Algorithm 1). We initialize two pixels as the central means of each group and assign the others following the condition $\hat{k} = \text{argmin}_{k=\overline{1,2}} d(p, \mu_k)$. $\hat{k}$ is the group index that the candidate pixel p is assigned to and μ_k is the central mean of group k. After all the pixels are assigned to the corresponding groups, we update the mean value and repeat the process until reaching the maximum number of iterations.

The PPG signal is obtained by taking the average of the intensity of the region. However, not all the pixels contribute to the signal equally; some are only noise. Therefore, to amplify the signal, a filtering procedure based on the characteristic of the PPG itself is applied. The phenomena of PPG signal is to describe the blood flow characteristic, thus, it should present some types of pulse waveform. In other words, their frequency should be bounded within the range of our heart beat. Given that information as a clue, we divide each segment into small cells and measure the frequency of each cell across the time. The sub-PPG signal generated by one specific cell will be converted into the frequency domain to detect the highest peak. If the dominant frequency lays in between the lowest and highest allowable heart rate, the cell is considered to belong to the interest region. Finally, we block only the regions that contain the pulsatile information.

PPG Extraction and Absorption Ratio Measurement. The PPG signal is obtained from the reflected lights are highly corrupted by noise especially in the region of NIR. Therefore, the signals need to go through a set of different layers of filtering to improve the SNR without distorting the shape of that signal. In our work, we apply the Savitzky-Golay filtering [54] which helps reduce the noise while still maintaining the pulsatile shape. The peak-to-peak measurement is used to estimate the AC component, and the DC is measured by the bottom of local PPG signal (Equation (7)).

7 MODEL FOR CAMERA-BASED INTENSITY TO SPO_2 LEVEL INFERENCE

Red Chromophore Influence Analysis and Compensation Approach. Recall that the absorptivity ratio R equals $\frac{AC(r)/DC(r)}{AC(ir)/DC(ir)}$. Let's denote $\frac{AC(r)}{DC(r)} = n$ and $\frac{AC(ir)}{DC(ir)} = d$; the ratio becomes $R = \frac{n}{d}$. Information

collected in both the numerator and the denominator is interfered with by the red chromophore coming from the skin, flesh, and blood. We introduce a compensation term for the red color to each part of the fraction. For each frame, the mean intensity of red channel for each filter is calculated and we note them as τ_r and τ_{ir}. To normalise the compensation value, we subtract the ratio to the mean red intensity of the whole image γ. Finally, the absorptivity ratio R with red chromophore compensation is presented as follows:

$$R = \frac{n - k_1\tau_{ir}}{d - k_2\tau_r} - k_3\gamma, \tag{11}$$

with k_1, k_2, and k_3 are the gain parameters to control how much each compensation term is involved in the equation. For convenience, we set $k_1 = k_2$ with the assumption that the τ_r and τ_{ir} have the same impacts on the ratio.

Non-Linear Calibration with RANSAC Outliers Removal. Absorption ratio estimation (R) is measured following the equation that has been proven by the Beer-Lambert law, as mentioned in Section 3. However, such derivation must be modified with the flashlight light source due to the impact of high saturation and large number of outliners. To overcome the problem, we propose a hybrid structure of using RANSAC [10] and the Levenberg-Marquardt (LM) [31] optimisation to obtain extinction coefficients. More specifically, given a derived model and a set of observation, LM is a gradient-based method which is usually used to estimate the unknown parameters/variables in the model. Our approach attempts to minimise the gap between the prediction values and the ground truth by updating the parameters following the slope of the gradient. To simplify the notation for the next step, we generalise the equation of approximating SpO_2 with input R (mentioned in Section 3) as follows:

$$S = \frac{a_H - b_H R}{a_H - a_O + [b_O - b_H]R}, \tag{12}$$

where a_O, a_H, b_O and b_H are the extinction coefficients of two wavelengths. In this case, finding the system model is similar to identify the values of a_O, a_H, b_O, and b_H given a set of input N pairs $\{s^i, R^i, i = \overline{1, N}\}$. We formulate the problem as an optimisation with $\beta = [a_0, a_H, b_O, b_H]$ are the unknown variables

$$\hat{\beta} = \underset{\beta}{\operatorname{argmin}} \sum_{i=1}^{N} \|s_i - S(\beta, R_i)\|. \tag{13}$$

We can derive the optimal solution for these variables by iteratively updating with a portion of gradient $\beta_{t+1} = \beta_t - \gamma \mathbf{J}_t$, where $\mathbf{J}_t = \frac{\partial S(\beta_t)}{\partial \beta_t} = [\frac{\partial S(a_O)}{\partial a_O} \frac{\partial S(a_H)}{\partial a_H} \frac{\partial S(b_O)}{\partial b_O} \frac{\partial S(b_H)}{\partial b_H}]$ is the Jacobian matrix [49]. The choice of step value γ has a critical impact on the performance. In the Levenberg and Marquardt model, the step variable, called γ, is a function of residuals as follows: $\gamma = (\mathbf{J}^T\mathbf{J} + \lambda I)^{-1}(\mathbf{J}^T r)$, where $r = \sum_{i=1}^{N} \|s_i - S(\beta, R_i)\|$ is the residual estimated at each iteration (T is the matrix transpose operator). The λI term makes sure that $\mathbf{J}^T\mathbf{J} + \lambda I$ is always invertible and lambda is the damping factor used to control the time of convergence. In practice, lambd can be set to equal to 1. Following this model, we optimise the extinction coefficients adopting the Lavenberg and Marquardt algorithm. In particular, we derive the Jacobian matrix by taking the partial derivative of each coefficient:

$$\begin{aligned} \mathbf{J} &= \left[\frac{\partial S(a_O)}{\partial a_O} \quad \frac{\partial S(a_H)}{\partial a_H} \quad \frac{\partial S(b_O)}{\partial b_O} \quad \frac{\partial S(b_H)}{\partial b_H} \right] \\ &= \left[\frac{(a_H - b_H R)}{g(\beta)} \quad \frac{(-a_O + b_O R)}{g(\beta)} \quad \frac{R(b_H R - a_H)}{g(\beta)} \quad \frac{R(a_O - b_O R)}{g(\beta)} \right], \end{aligned} \tag{14}$$

ALGORITHM 2: Extinction coefficients estimation-based Levenberg-Marquardt optimization.

input: $s, R, MaxIte, \epsilon, \lambda$- The set of ground truth SpO_2, the absorption ratio R, maximum number of iteration, minimum error and the damping factor.
output: $\hat{\beta}$- The optimal four coefficients $\hat{\beta} = [\hat{a_0}, \hat{a_H}, \hat{b_O}, \hat{b_H}]$

Initialise values for β_0 according to the expected wavelength.
/* Finding the optimal β.*/
for $t = 0 \rightarrow MaxIte$ **do**
  $r_t \leftarrow \sum_{i=1}^{N}(s_t^i - S(\beta_t, R^i))$
  $\mathbf{J}_{t+1} \leftarrow \frac{\partial S(\beta_t, R)}{\partial \beta_t}$ following Equation (14)
  $\beta_{t+1} \leftarrow \beta_t + (\mathbf{J}^T\mathbf{J} + \lambda I)^{-1}(\mathbf{J}^T r)$
  if $r < \epsilon$ **then**
    break;
  end
end
return β_t;

ALGORITHM 3: RANSAC optimization-based Levenberg-Marquardt model.

input: $s, R, k, MaxIte$- The set of ground truth SpO_2, the absorption ratio R, the minimum number to be inlier set and the maximum iterations.
output: $\hat{\beta}$- The optimal four coefficients $\hat{\beta} = [\hat{a_0}, \hat{a_H}, \hat{b_O}, \hat{b_H}]$

Initialise values for $\hat{\beta}$/* Finding the optimal β.*/
for $t = 0 \rightarrow MaxIte$ **do**
  /* Sampling a subset and verify possible inliers.*/
  $X = \{s^q, R^q, q = \overline{1, K}\} \leftarrow$ SubSamplingPoints(s, R)
  $\hat{\beta}_t \leftarrow$ Levenberg_Marquardt_Opt(X) using Algorithm 2
  $I_t \leftarrow$ Validate($\hat{\beta}_t, \{s, R\}/\ X$)
  if $\|I_t\| > k$ **then**
    /* We may find a good model.*/
    $e_t \leftarrow$ ValidateError(β_t, s, R)
    if $e_t < \hat{e}$ **then**
      $\hat{\beta} \leftarrow \beta_t, \hat{e} \leftarrow e_t$
    end
  end
end
return β_t;

where $g(\beta) = (a_H - a_O + (b_O - b_H)R)^2$. We summarise the process of estimating the four coefficients as in Algorithm 2.

Recall that we are using components in off-the-shelf smartphone, i.e., flashlight and embedded camera sensor, this results in intensive noises into our system. Thus, not all the pairs of s_i, R_i are cooperative. Some of the pairs are redundant and therefore reducing the accuracy of estimation. More importantly, as there is no prior information about the relation between s and R, blindly justifying which pairs are useful for the model is one of the directions. However, such an approach cannot provide an optimised solution. Instead, we indirectly measure the information that each data point contributes to the existing model. Then, we choose those pairs that have highest

Table 1. Demographic Description of Participants

Participant Demographics	
Age (years)	25–32 years old
Oxygen Saturation (%)	82–97
Gender Ratio	3 male: 3 female
Ethnicity	Asian: 4, White: 2

contribution as the inliers. Such technique is called RAndom SAmple Consensus (RANSAC). We adopt this technique for our model and present the procedure as in Algorithm 3.

To summarise, a subset of data is randomly withdrawn from the whole dataset and proceeds to the Lavenberg-Marquardt optimisation to obtain the possible coefficients. Then, we select points that are less than 2% of error to be possible iniliers. If the total number of possible inliers is less than a predefined k, it is qualified to compare with existing model with the input is the whole dataset. The final output will have the smallest error among those candidates.

8 PERFORMANCE EVALUATION

In this section, we first present key results of performing the real-time SpO_2 measurement using PhO_2 system. Next, we evaluate the sensitivity of PhO_2 to extract the usable and reliable PPG signal from the images captured by the smartphone's camera. By deploying the mobile application, we further illustrate the physical efficiency of our proposed system in terms of power consumption and processing time. Finally, we analyse the surveying of the users' experience of using the PhO_2 system to measure their SpO_2 level.

8.1 Experimental Methodology

To evaluate the performance of the PhO_2 pulse oximetry system, we conducted our experimental studies in a normal office environment and in hospitals. The light source is supplied by the phone's built-in flash with noise coming from the incandescent lights in the room. The participant demographics of our in-lab experiment can be found in Table 1.

We tested our system (PhO_2) altogether with (1) an FDA-approved, official in-hospital device (Nellcor PM10N [37]), (2) a cheap fingertip pulse oximeter (FACELAKE CMS50E [7]), (3) Digidoc app [15] on iPhone 6, and (4) iCare Health Monitor app [18] on Samsung Galaxy S5.

The Nellcor PM10N is provided by Children's Hospital Colorado with the password for full access to measure and manipulate patients' data. Nellcor is one of the pioneer brands in manufacturing pulse oximeters and has been frequently used as ground truth evidence [9, 13, 30, 51]. Therefore, the device is creditable for giving baseline measurements in our experiments. On the other hand, the two mobile applications on iOS and Android only provide discrete measurement, thus the recorded data were noted down and aligned manually for the sake of comparison. This experiment is tested on six subjects with various ages, ethics and genders. Each subject is asked to follow a clinical instruction of breathing sequence in order to correctly reduce the blood oxygen level, in which they are asked to exhale and inhale heavily for six consecutive times and hold their breath up to their limitation. The exhale and inhale sequences help to release most of the air from the lung, thus the SpO_2 reduction process in the subjects' body can be observed easily. The whole process takes thirty minutes and is repeated five times. The oxygen level of the subject is measured simultaneously using our PhO_2 and the four devices described above (Figure 11 shows the setup of all devices on the subject's fingers). In the second phase of project, we successfully deliver our prototype (Figure 12) to be tested in the hospital with real patients.

Fig. 11. Experiment setup to compare PhO_2 with other four pulse oximeters.

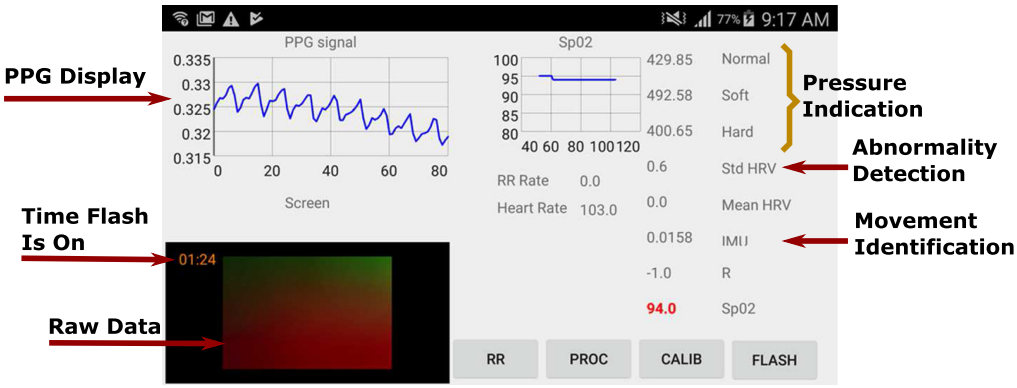

Fig. 12. Overview of the *PhO2* prototype including functions of detecting abnormal PPG signal, movement detection and pressure level indication.

To evaluate the effectiveness of new design in reducing heat from the flashlight, we use thermocouple and hand-multimeter (Figure 13) to measure heat draining from three different designs: single large tunnel, single small tunnel, and light distribution with and without optic bandpass filter.

8.2 PhO_2 System Performance

In-Lab Testing. In this section, we evaluate the performance of PhO_2 within six subjects and report the results comparing with the Nellcor PM10N. The experimental methodology is presented in an earlier section (Section 8.1). For each subject, we record data continuously and report the result for every second. As a result, 6 subjects account for 434 data points in total. Figure 14 presents the fine-grained SpO_2 predictions generated by PhO_2 for each subject. The evaluation results show that PhO_2 not only produces small error rates of SpO_2 level measurement but also illustrates the trend of oxygen level. This level of detail has not been addressed with most of the current smartphone-based approaches. The trend of oxygen level predicted by our system (blue line) is similar to the measurement of Nellcor device. For example, in the case of the measurement of the fifth subject, the estimated results by ground truth device starts at 96% and then goes up to 99%. Meanwhile,

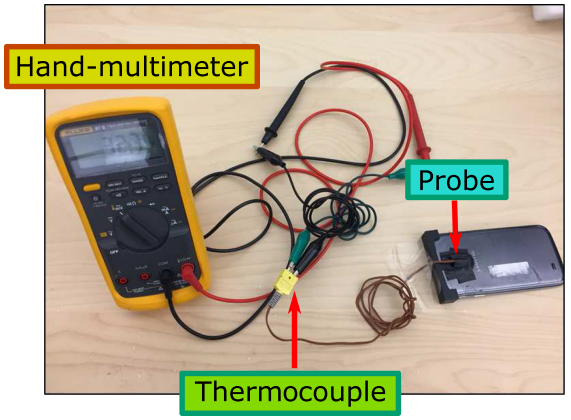

Fig. 13. Measuring heat coming out of the add-ons.

our system reports from 94% to 98%. In the last case, the subject drops the oxygen level to below 82%, which is the same as our prediction. The interesting point is that our system responds faster than the ground truth because when the subject performs the hyperventilating and begins to hold his/her breath, the oxygen level decreases right after that; when the subject starts to inhale, the oxygen level increases. The patterns of results show that our system can predict and follow the tendency of the SpO_2 level strictly even when oxygen level changes significantly.

Figures 15(a) and 15(b) summarise the evaluation of our system with respect to all subjects (each individual and general in total). The system can measure the level of oxygen with 80th percentile error less than 3.5%. The mean and standard deviation of the absolute error rate are 2.5% and 1.62%, respectively. The mean absolute error rate is similar to that of well-known pulse oximeters, which were reported to give the prediction with 2% of mean absolute error at normal condition [63]. In addition, the standard deviation of absolute error rate achieved by PhO_2 can be reduced by averaging together many measurements over a period of time, before any decision would be made about a patient's condition. Therefore, the error rate of our system is sufficient for a home care device which does not need very high accuracy. In some cases, physicians are only concerned when it is below a certain threshold. For example, the Pediatric Asthma Score [50] identifies patients as Severe if their blood oxygen level is lower than 90%. In addition, to have a better view on the system performance, we conduct the test of Kendall correlation coefficients between prediction and ground truth. Figure 15(c) displays the result with Kendall's τ equal to 0.72 showing that the two variables are relatively matched. To avoid a dense cluster of points, we only mark a few data samples in Figure 15(c) by a plus sign for illustration. In details, from subject 1 to 5, the error rate is stable and close to the general case. This group of subjects includes different races, ages, and genders, but their demographic characteristics do not affect our system function. In fact, the factors that can affect the system from our observation is contact pressure and sensitivity of the system with respect to light condition. Contacting pressure is managed by pressure detection algorithm and the change of light environment is handled by the ROI detection and the design of our add-on.

The existing apps, on the other hand, represented by Digidoc (iOS) and iCare Health Monitor (Android) show their performance in Figure 16 with all subjects evaluated in our system and the groundtruth is captured by the Nellcor device. The mean absolute error of Digidoc and iCare Health Monitor are 5% and 4.36%, respectively. The results clearly explain how the apps would fail to keep track on low oxygen levels. Moreover, unlike the PhO_2, they only operate as a one-time measurement and thus, are unable to present continuous records.

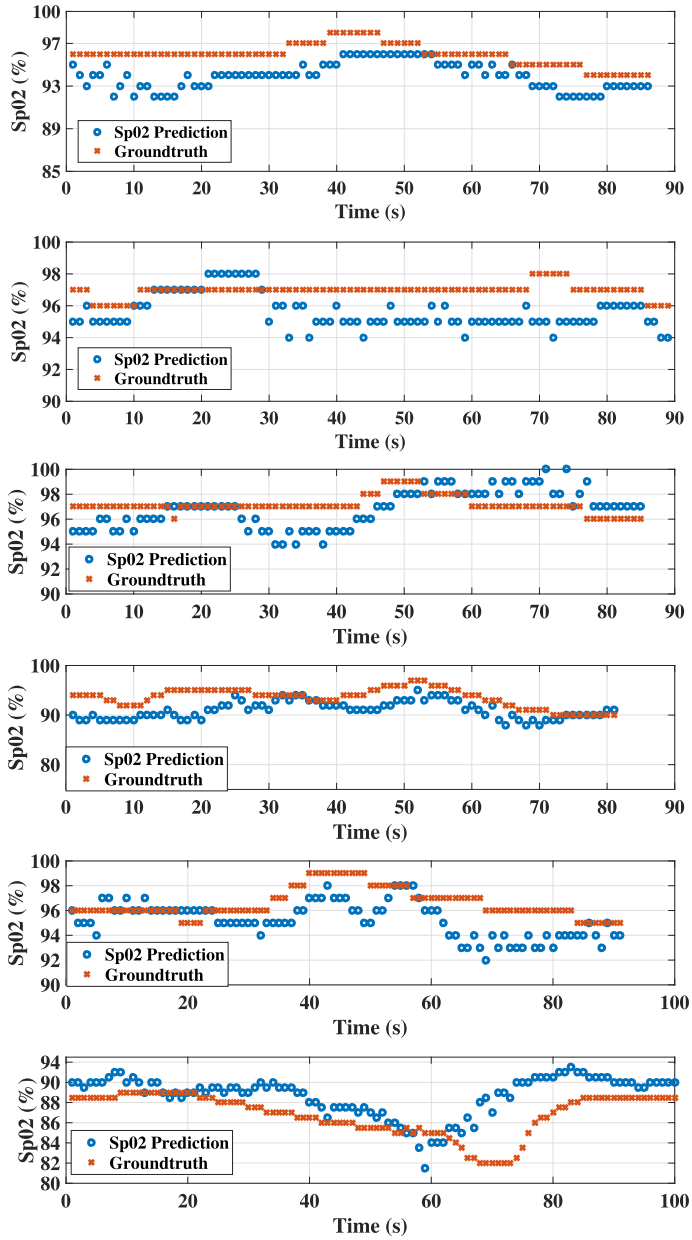

Fig. 14. Fine-grained evaluation on prediction of oxygen level of six participants.

Evaluation in the Hospital. We present our results for the experiments in the hospital with six patients. The prediction ranges from 85% to 94% and the Kedall correlation is 0.83 (Figure 17), showing that our system can perform well in practical scenarios. We continuously measured data on each patient and reported the result for every second. Over all, we received 611 data points in total. Figure 18 illustrates the fine-grained detection for each patient. Even though the prediction fluctuated more than the in-lab experiment, it still followed the trend of the oxygen saturation level. The primary cause of this fluctuation is due to the body movement. Our subjects in the

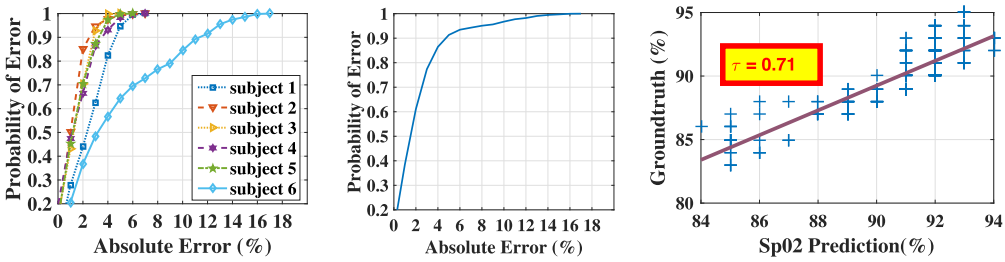

(a) CDF of each participant (b) CDF of the whole dataset (c) Kendall rank correlation coefficient between PhO_2 and ground-truth.

Fig. 15. Performance evaluation of the in-lab experiment.

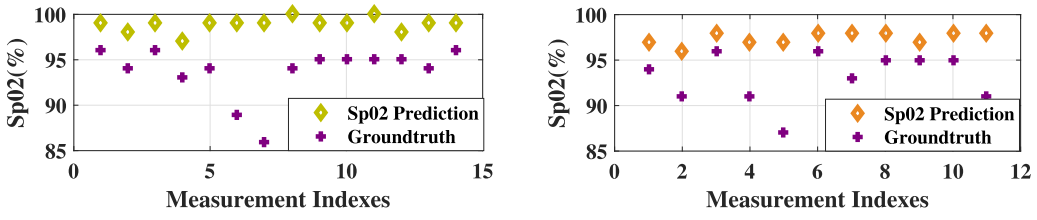

(a) DigiDoc (iOS) (b) iCare Health Monitor (Android)

Fig. 16. Performance evaluation of two representative applications.

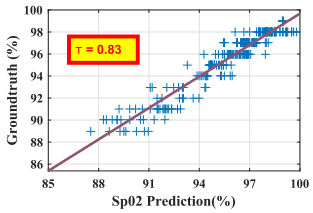

Fig. 17. Kendall rank correlation coefficient between PhO_2 and ground-truth of the in-hospital evaluation.

hospital were mostly children, hence, usually were more active than the adults. The COMIRB 17-1180 for this study was reviewed and approved under the requirements of the pre-2018 version of the Federal Policy for the Protection of Human Subjects. The participants could not perform the breath holding. Therefore, we had to look for the hypoxia patients whose oxygen saturation level could drop below 90%. If they were children, their parent/guardian needed to read and sign the consent. We cleaned our PhO_2 and the ground truth devices using sanitizer wipes before and after the evaluation to prevent the spread of infectious diseases.

8.3 Sensitivity Analysis with In-Lab Evaluation

Impact of Wavelength Selection. Since our primary goal is to provide evidence that combining different layers of filters can extract the desired NIR lights. This section aims to assist our justification. Relying on the natural phenomena of gradient descent is all about the search for the local maxima in the set of possible solution. Obviously, the initial solution is the factor that helps to define the performance of the optimisation. Our purpose of conducting the experiment is to look for the relation between the optimal solution and the wavelength selection. The expectation relies on the fact

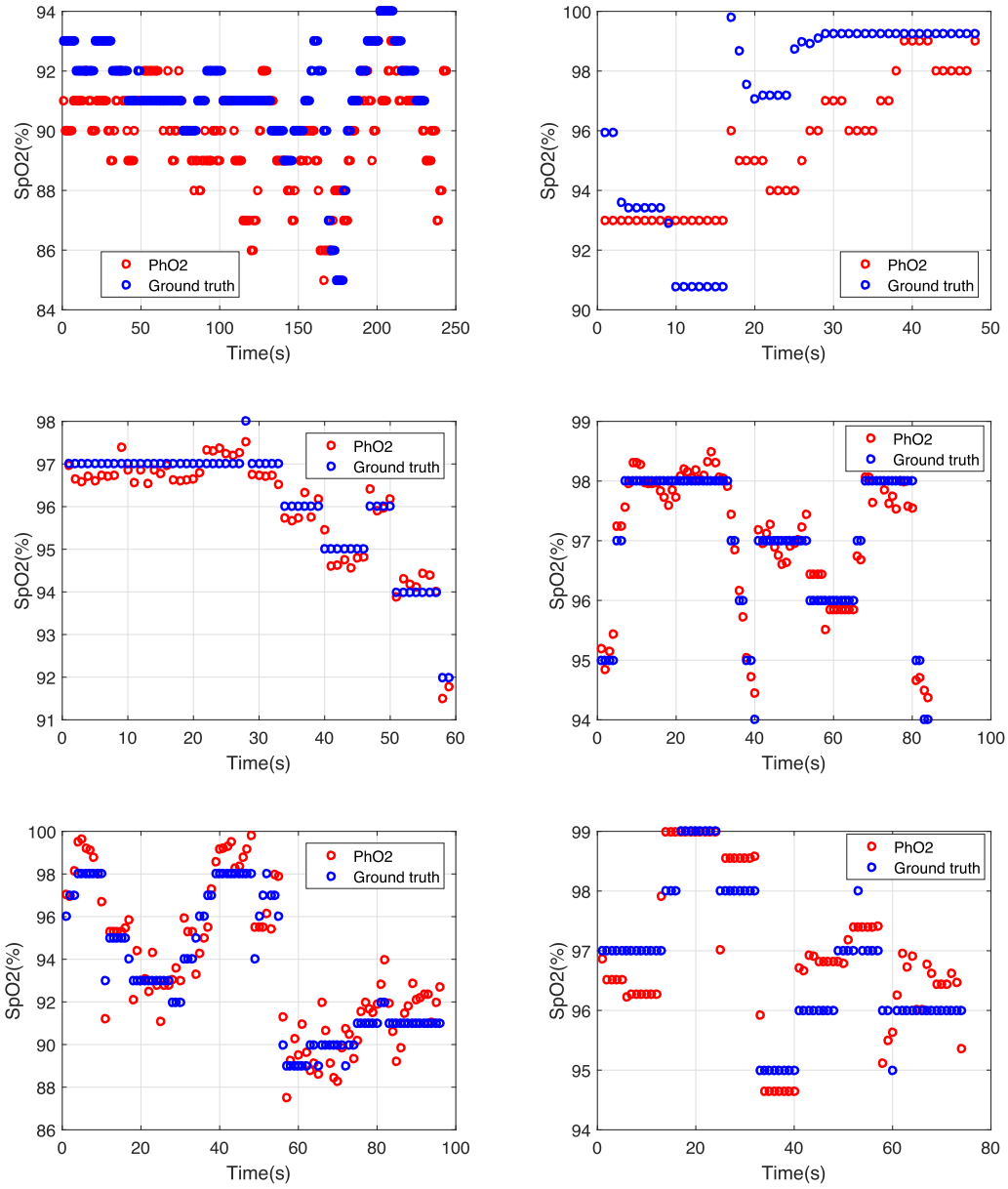

Fig. 18. Performance evaluation of experiments in hospital.

that only NIR wavelengths aligning with our optimisation model can provide a high prediction. Starting at 610 nm and going down to 602 nm, the performance gradually decreases as shown in Figure 21 which satisfies our assumption. The lights captured in that region cannot be the visible lights since those wavelengths are reasonably fails to predict the oxygen level. In addition to the optimisation model, the linear calibration shows its limited capability in dealing with high complex problems. Specifically, Figure 22 shows that the average accuracy linear calibration is about 94% while the one with non-linear calibration can serve up to 97%. By looking at the CDF function,

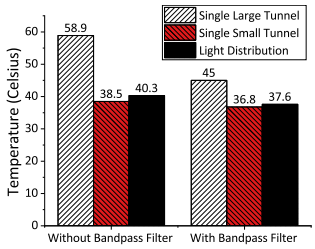

Fig. 19. Experiments of heat at the finger using different designs.

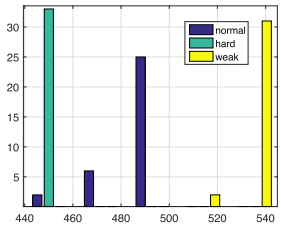

Fig. 20. Hardness of the fingertip pressed on the PhO_2 add-on for one subject.

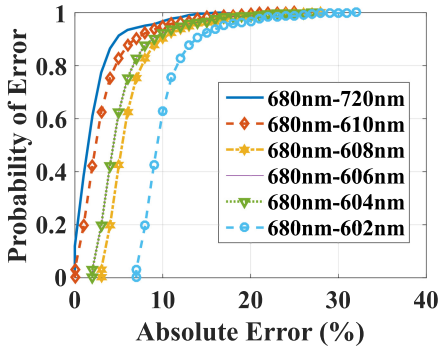

Fig. 21. Results of selecting different pairs of wavelength.

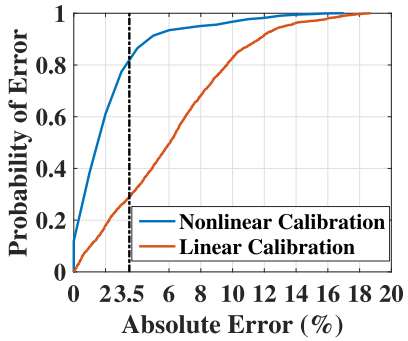

Fig. 22. Comparison between linear and non-linear calibration in term of system performance.

the efficiency of nonlinear calibration is even more remarkable since the confidence level of the linear model to achieve an error rate less than 3% is only 10%.

Mitigating Users' Pressure Issue. We collected data for the pressure hardness level from seven subjects. Each subject was asked to record multiple videos with different finger postures while using PhO_2. Each video was processed by pressure detection algorithm (described in Section 6.1) in order to classify each video frame into one of three pressure states. Figure 20 shows the mean and distribution of calculated variance of Laplacian Image of each frame from one subject. The results of the mean values between each of three states are clearly distinct. The algorithm can process for every frame and in real-time.

Alleviate Phone's Flashlight Heat. The original design without optic filter can heat up to 58.9 degrees Celsius, while the light distribution is only around 40.3 degrees as shown in Figure 19. Including the optic filter, the heat drops down to 37.6 degrees with the light distribution design. In general, the optic filter helps to keep the temperature low because the strong energy wavelengths as UV are filtered out. The light distribution functions, as we expected, to avoid skin burn.

8.4 User Experience Survey

We asked the subjects to take a survey about their experience of using our PhO_2 prototype after their experiment period. Specifically, our questionnaire concentrated on the comfort, safety, and

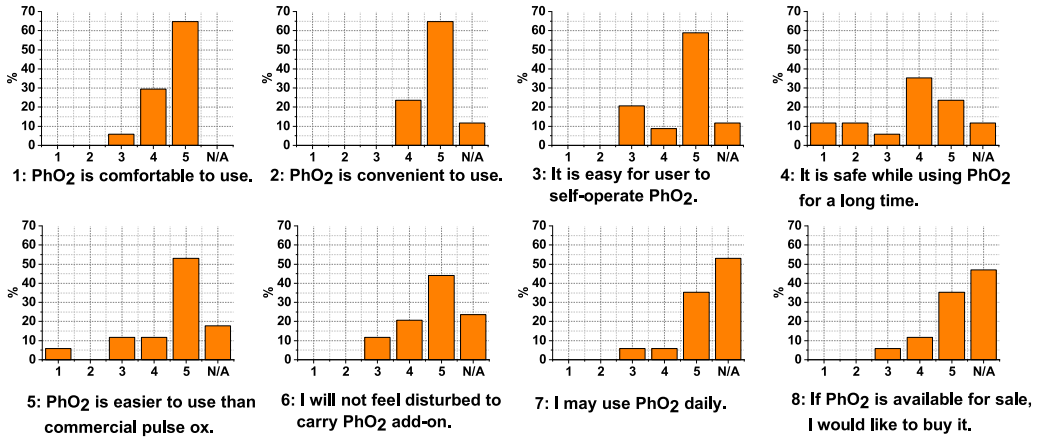

Fig. 23. User Experience Questionnaire Results.

the usability of the device. Figure 23 shows all the questions and their results. The scale is from 1 to 5 corresponding to "Strongly Disagree" to "Strongly Agree", respectively.

Overall, the results show the users' agreement of being highly satisfied to use PhO_2 for the SpO_2 level measurement. The reason given is because PhO_2 is friendly to use, quick to operate, and lightweight to carry. Also, 6 in 12 subjects stated that our PhO_2 provides more comfort than the existing commercial pulse oximeters. However, some of them raised their concern about the high temperature generated from the flashlight after 10 minutes of continuously turning it on as well as placing their fingertip on it. We believe that this concern will be eliminated in real-life scenarios when PhO_2 is used in less than 5 minutes for each time of measurement. Over all, the user study showed the possibility and promise of our PhO_2 device to be adopted by users who require a management of their SpO_2.

9 DISCUSSIONS

Limitations. The first limitation is the long initialisation delay of the system. In the current design, PhO_2's algorithms introduce undesirable delays to approximate the ROI, estimating pressure, and SpO_2 measurement. With our current setup, the ROI takes 6 seconds, pressure detection requires 1 second, and SpO_2 measurement requires 6 seconds of data. This meant that the system will not be able to output results for the first 12 seconds before it can monitor the SpO_2 level continuously. Second, we only could collect data from 12 participants due to the current IRB limitation. We are developing new IRB protocol to perform an extensive study with $n = 60$ subjects to evaluate PhO_2 using hypoxia procedure (i.e., bringing the oxygen level of a subject gradually down from normal range (95%–100%) down to extremely low range (65%–70%)) for validation. Last, we have only tested PhO_2 on limited number of smartphone devices. Though the device-to-device variations are considered from the design of our system, we would expect variations in the accuracy on different hardware. Future study will include a much broader range of devices with different diode for flashlight and camera supplier.

Potential Phone Case Design. Even though the current design is a plug-n-play prototype, we intend to build a phone case that will always be attached to the phone. The phone case includes a sliding filter that allows switching between the normal camera usage and measuring SpO_2 level based on PhO_2 model. Since our design is power free and compact, users can measure the oxygen

saturation level any time, unlike normal pulse oximeters which require an external power source to support the LEDs and their circuit.

Future Applications. The techniques developed in this article have a potential to apply to other sensing domains such as substance detection using mobile phone flashlight and camera. For example, the same technique might potentially benefit anemia diagnosis and skin disease detection. The ability to collect SpO_2 might allow PhO_2 to be used for cardiopulmonary disease (e.g., heart failure and congenital heart disease have changed in oxygen level). More significantly, as monitoring SpO_2 levels is clinically standard for screening chronic respiratory diseases and assessing their severity, our PhO_2 system can be used as a lightweight solution for chronic patients to check their SpO_2 level periodically. Additionally, by doing such the periodic SpO_2 check, our system can further predict the upcoming health problem (e.g., asthma) and quickly react against the patient's health situation, which begins getting worse. For instance, the mobile app can automatically activate a call to a medical doctor for a confirmation of his/her saturation level drops. As a result, from those who need Telehealth monitoring, our PhO_2 system can provide cost-effective strategy to support the clinical routine to follow up the patients. In addition to being mobile, smartphones are ubiquitous and this technology could potentially bring this key clinical physical finding to the global communities which are unable to purchase standard pulse ox technology due to the cost or logistic constraints (e.g., third-world countries or remote geographical areas). Finally, not only working independently, our proposed techniques can further be integrated into existing low-cost sensing systems such as the in-ear physiological sensor developed in [38] to provide additional data sources, which is useful for improving their prediction performance.

10 CONCLUSIONS

In this article, we presented PhO_2, a phone-based oxygen level estimation system using COTS phone's camera and flashlight. Since the smartphones' camera and flashlight are not designed for this purpose, it leads to a number of challenges including the lack of IR light from the flashlight, the lack of a mathematical model to convert camera-based intensity ratio to SpO_2 level, the noisy signal captured by the camera, the unstable and undesirable pressure at the users' finger contact area and the strong heat generated by the flashlight. We provide a careful hardware design and a set of algorithms to overcome these challenges and making phone-based non-invasive SpO_2 level measurement possible. We also conducted a set of experiments to evaluate the performance of PhO_2. The evaluation results showed that PhO_2 obtained high performance of 3.5% of estimation accuracy which is considered clinically sufficient by FDA standards. Also, the experiments in the hospital achieve high correlation with the ground-truth with Kendall τ equalling 0.83/1.0. Last, we discussed the limitations of the current system, identifying its potential extension and future workand highlighted the PhO_2 potential applications.

ACKNOWLEDGMENTS

The authors express their appreciation to Prof. Hieu Nguyen, New Jersey Institute of Technology and Mr David Alchenberger, JILA-Keck Lab for helping with the measurement of the phone flashlight's and optical filters' spectrum.

REFERENCES

[1] 680nm Filter 2017. Visible Bandpass Filter—680nm FWHM 10nm. https://goo.gl/PhLd8x.
[2] Geeta S. Agashe, Joseph Coakley, and Paul D. Mannheimer. 2006. Forehead pulse oximetryheadband use helps alleviate false low readings likely related to venous pulsation artifact. *Anesthesiology* 105, 6 (2006).
[3] BCI WW1000 2017. BCI WW1000 Spectro2 Hand Held Pulse Oximeter with Ear Clip Sensor. https://goo.gl/xPsw1F.
[4] John W. Berkenbosch and Joseph D. Tobias. 2012. Comparison of a new forehead reflectance pulse oximeter sensor with a conventional digit sensor in pediatric patients. *Respiratory Care* 51, 7 (2012), 726–731.

[5] J. Brimacombe, C. Keller, and J. Margreiter. 2000. A pilot study of left tracheal pulse oximetry. *Anesth. Analg.* 91, 4 (2000), 1003–1006.
[6] Nam Bui, Anh Nguyen, Phuc Nguyen, Hoang Truong, Ashwin Ashok, Thang Dinh, Robin Deterding, and Tam Vu. 2017. PhO2: Smartphone based blood oxygen level measurement systems using near-IR and RED wave-guided light. In *Proceedings of the 15th ACM Conference on Embedded Network Sensor Systems CD-ROM*. ACM, 230–244.
[7] CMS-50E 2017. CMS-50E OLED Fingertip Pulse Oximeter. https://goo.gl/Fmncr5.
[8] Steve Cunningham and Ann McMurray. 2006. The availability and use of oxygen saturation monitoring in primary care in order to assess asthma severit. *Primary Care Respiratory Journal* 15 (2006), 98–101.
[9] Marco Fernandez, Kathy Burns, Beverly Calhoun, Saramma George, Beverly Martin, and Chris Weaver. 2007. Evaluation of a new pulse oximeter sensor. *American Journal of Critical Care* 16, 2 (2007), 146–152.
[10] M. A. Fischler and R. C. Bolles. 1981. Random sample consensus: A paradigm for model fitting with applications to image analysis and automated cartography. *Comm. of the ACM* 24 (1981), 381–395.
[11] Sotirios Fouzas, Kostas N. Priftis, and Michael B. Anthracopoulos. 2011. Pulse oximetry in pediatric practice. *Pediatrics* 128, 4 (2011), 740–752.
[12] Matthew J. Hayes and Peter R. Smith. 1998. Artifact reduction in photoplethysmography. *Applied Optics* 37, 31 (Nov 1998), 7437–7446.
[13] Jeffrey M, Haynes. 2007. The ear as an alternative site for a pulse oximeter finger clip sensor. *Respiratory Care* 52, 6 (2007), 727–729.
[14] Heart Rate Pulse Oximeter 2017. Heart Rate Pulse Oximeter. https://goo.gl/nZWuqU.
[15] Kelly Hodgkins. 2014. Daily app: Digidoc pulse oximeter tries to measure your heart rate and oxygen levels. *Modern Healthcare* (2014).
[16] Homedics 2017. Homedics Px-100 Deluxe Pulse Oximeter. https://goo.gl/qaomPz.
[17] Cheng-Yang Huang, Ming-Che Chan, Chien-Yue Chen, and Bor-Shyh Lin. 2014. Novel wearable and wireless ring-type pulse oximeter with multi-detectors. *Sensors* 14, 9 (2014), 17586–17599.
[18] iCare Oxygen Monitor 2017. iCare Oxygen Monitor. https://goo.gl/E9RGoU.
[19] Instant Pulse Oximeter 2017. Instant Pulse Oximeter. https://goo.gl/0O59Qx.
[20] Instant Pulse Rate 2017. Instant Pulse Rate. https://goo.gl/B3FnkT.
[21] Invasive Blood Test 2017. Invasive Tests and Procedures. https://goo.gl/sKxCYB.
[22] iPhone6 Camera Lens 2017. iPhone 6 camera megapixels and photo samples. https://goo.gl/ppB0xZ.
[23] Priya Jegatheesan, Dongli Song, Cathy Angell, Kamakshi Devarajan, and Balaji Govindaswami. 2013. Oxygen saturation nomogram in newborns screened for critical congenital heart disease. *Pediatrics* 131, 6 (2013), e1803–e1810.
[24] Christina Jørgensen and Toke Bek. 2014. Increasing oxygen saturation in larger retinal vessels after photocoagulation for diabetic retinopathy. *Investigative Ophthalmology & Visual Science* 55, 8 (2014), 5365.
[25] Christian Kanzow, Nobuo Yamashita, and Masao Fukushima. 2004. Levenberg-Marquardt methods with strong local convergence properties for solving nonlinear equations with convex constraints.*J. Comput. Appl. Math.* 172, 2 (2004), 375–397.
[26] W. Karlen, J. Lim, J. M. Ansermino, G. Dumont, and C. Scheffer. 2012. Design challenges for camera oximetry on a mobile phone. In *Proceedings of the 2012 Annual International Conference of the IEEE Engineering in Medicine and Biology Society* (2012).
[27] J. G. Kim and H. Liu. 2007. Variation of haemoglobin extinction coefficients can cause errors in the determination of haemoglobin concentration measured by near-infrared spectroscopy. *Physics in Medicine and Biology* 52, 20 (2007), 6295.
[28] F. Lamonaca, D. L. Carnì, D. Grimaldi, A. Nastro, M. Riccio, and V. Spagnolo. 2015. Blood oxygen saturation measurement by smartphone camera. In *Proceedings of the 2015 IEEE International Symposium on Medical Measurements and Applications (MeMeA)*.
[29] LEE Filter 2017. LEE Filters 738 JAS GREEN. https://goo.gl/zLodlp.
[30] Michael S. Lipnick, John R. Feiner, Paul Au, Michael Bernstein, and Philip E. Bickler. 2016. The accuracy of 6 inexpensive pulse oximeters not cleared by the Food and Drug Administration: The possible global public health implications. *Anesthesia & Analgesia* 123, 2 (2016), 338–345.
[31] Manolis I. A. Lourakis. 2005. A brief description of the Levenberg-Marquardt algorithm implemented by LEVMAR. *Foundation of Research and Technology* 4 (2005), 1–6.
[32] Suzanne Low, Yuta Sugiura, Dixon Lo, and Masahiko Inami. 2014. Pressure detection on mobile phone by camera and flash. In *Proceedings of the 5th Augmented Human International Conference (AH'14)*. 11:1–11:4.
[33] Emin Maltepe and Ola Didrik Saugstad. 2009. Oxygen in health and disease: Regulation of oxygen homeostasis-clinical implications. *Nature Reviews Molecular Cell Biology* 65 (2009), 261–268.
[34] Robert McMillan. 2014. These medical apps have doctors and the FDA worried. https://goo.gl/rEXYGD.

[35] Sanjay V. Mehta, Patricia C. Parkin, Derek Stephens, and Suzanne Schuh. 2004. Oxygen saturation as a predictor of prolonged, frequent bronchodilator therapy in children with acute asthma. *The Journal of Pediatrics* 145, 5 (2004), 641–645.
[36] Payal Modi, Richard B. Mark Munyaneza, Elizabeth Goldberg, Garry Choy, Randheer Shailam, Pallavi Sagar, Sjirk J. Westra, Solange Nyakubyara, Mathias Gakwerere, Vanessa Wolfman, Alexandra Vinograd, Molly Moore, and Adam C. Levine. 2013. Oxygen saturation can predict pediatric pneumonia in a resource-limited setting. *The Journal of Emergency Medicine* 45, 5 (2013), 752–760.
[37] Nellcor™2017. Nellcor™Portable SpO_2 Patient Monitoring System, PM10N. https://goo.gl/bxWG7R.
[38] Anh Nguyen, Raghda Alqurashi, Zohreh Raghebi, Farnoush Banaei-kashani, Ann C. Halbower, and Tam Vu. 2016. A lightweight and inexpensive in-ear sensing system for automatic whole-night sleep stage monitoring. In *Proceedings of the 14th ACM Conference on Embedded Network Sensor Systems CD-ROM*. ACM, 230–244.
[39] NIR filter 2017. NIR filter thinkness. https://goo.gl/IkPedL.
[40] M. Nitzan, A. Romem, and R. Koppel. 2014. Pulse oximetry: Fundamentals and technology update. *Medical Devices: Evidence and Research* 7 (2014), 231–239.
[41] NONIN 2017. NONIN 8000Q2 Ear Clip Sensor. https://goo.gl/P2a9W1.
[42] Optical Spectrum Analyzer 2017. Ando Model AQ6315E Optical Spectrum Analyzer. https://goo.gl/apKy2C.
[43] OxiMax 2017. Nellcor OxiMax D-YSE Ear Clip Sensor. https://goo.gl/Wajkva.
[44] Oximetry.org 2017. History of pulse oximeter. https://goo.gl/y0Mm7.
[45] Christian L. Petersen, Tso P. Chen, J. Mark Ansermino, and Guy A. Dumont. 2013. Design and evaluation of a low-cost smartphone pulse oximeter. *Sensors* 13, 12 (2013), 16882–16893.
[46] C. L. Petersen, H. Gan, M. J. MacInnis, G. A. Dumont, and J. M. Ansermino. 2013. Ultra-low-cost clinical pulse oximetry. In *Proceedings of the 2013 35th Annual International Conference of the IEEE Engineering in Medicine and Biology Society (EMBC)*.
[47] Pinhole size. 2017. Camera pinhole size. https://goo.gl/S0Bi4c.
[48] Quest Q1911. 2017. Quest Q1911 3-in-1 Pulse Oximeter. https://goo.gl/eubKLf.
[49] Osbaldo Resendis-Antonio. 2013. Jacobian Matrix. In *Encyclopedia of Systems Biology*. 1061–1062.
[50] Safety and Quality Collaborative Asthma Management Pathway (ED and IP) 2017. Children's Hospital Association of Texas Safety and Quality Collaborative Asthma Management Pathway (ED and IP). https://goo.gl/vN676X.
[51] Lynn Schallom, Carrie Sona, Maryellen McSweeney, and John Mazuski. 2007. Comparison of forehead and digit oximetry in surgical/trauma patients at risk for decreased peripheral perfusion. *Heart & Lung: The Journal of Acute and Critical Care* 36, 3 (2007), 188–194.
[52] Scott Prahl. 1998. Tabulated molar extinction coefficient for hemoglobin in water. Retrieved on 2017 from https://goo.gl/7SBwzQ.
[53] C. G. Scully, J. Lee, J. Meyer, A. M. Gorbach, D. Granquist-Fraser, Y. Mendelson, and K. H. Chon. 2012. Physiological parameter monitoring from optical recordings with a mobile phone. *IEEE Transactions on Biomedical Engineering*, 303–306.
[54] Mary C. Seiler and Fritz A. Seiler. 1989. Numerical recipes in C: the art of scientific computing. *Risk Analysis* 9, 3 (1989), 415–416.
[55] M. C. Simon and B. Keith. 2008. The role of oxygen availability in embryonic development and stem cell function. *Nature Reviews Molecular Cell Biology* 9 (2008), 285–296.
[56] SM-165. 2017. Santamedical Generation 2 SM-165 Fingertip Pulse Oximeter Omximetry Blood Oxygen Saturation Monitor with carrying case, batteries and lanyard. https://goo.gl/vi2ZLz.
[57] Kendric C. Smith. 1991. The photobiological basis of low level laser radiation therapy. *Laser Therapy* 3, 1 (1991), 19–24.
[58] SolidWorks. 2017. SOLIDWORKS. http://www.solidworks.com/.
[59] Norbert Stubán and Niwayama Masatsugu. 2008. Non-invasive calibration method for pulse oximeters. *Periodica Polytechnica Electrical Engineering* (2008), 91–94. DOI: https://doi.org/10.3311/pp.ee.2008-1-2.11
[60] Sarah Sykes, Ruth Kingshott, and Robert Primhak. 2011. Awake and asleep oxygen saturations in infants with chronic neonatal lung disease. *Acta Paediatrica* 100, 8 (2011), 1087–1091.
[61] Vigor Sp02., 2017. Vigor Sp02. https://goo.gl/MFfsTJ.
[62] Edward Jay Wang, William Li, Doug Hawkins, Terry Gernsheimer, Colette Norby-Slycord, and Shwetak N. Patel. 2016. HemaApp: Noninvasive blood screening of hemoglobin using smartphone cameras. In *Proceedings of the 2016 ACM International Joint Conference on Pervasive and Ubiquitous Computing (UbiComp'16)*. 3320–3338.
[63] A. C. Ralston, R. K. Webb, and W. B. Runciman. 1991. Potential errors in pulse oximetry. II. Effects of changes in saturation and signal quality. *Anaesthesia* 46, 3 (1991), 207–212.
[64] S. Wendelken, S. McGrath, G. Blike, and M. Akay. 2004. The feasibility of using a forehead reflectance pulse oximeter for automated remote triage. In *Proceedings of the IEEE 30th Annual Northeast Bioengineering Conference, 2004.* 180–181.

[65] J. Xiong, L. Cai, D. Jiang, H. Song, and X. He. 2016. Spectral matrix decomposition-based motion artifacts removal in multi-channel PPG sensor signals. *IEEE Access* 4 (2016), 3076–3086.
[66] Y. S. Yan and Y. T. Zhang. 2008. An efficient motion-resistant method for wearable pulse oximeter. *IEEE Transactions on Information Technology in Biomedicine* 12, 3 (2008), 399–405.
[67] Jianchu Yao and S. Warren. 2004. A novel algorithm to separate motion artifacts from photoplethysmographic signals obtained with a reflectance pulse oximeter. In *Proceedings of the 26th Annual International Conference of the IEEE Engineering in Medicine and Biology Society*, Vol. 1. 2153–2156.
[68] W. G. Zijlstra, A. Buursma, and W. P. Meeuwsen-van der Roest. 1991. Absorption spectra of human fetal and adult oxyhemoglobin, de-oxyhemoglobin, carboxyhemoglobin, and methemoglobin. *Clinical Chemistry* 37, 9 (1991), 1633–1638.

Received February 2018; revised April 2019; accepted August 2019